Macromolecules

pubs.acs.org/Macromolecules Article

Conjugated Ladder Poly(thienobenzothiazine): Synthesis, Electronic Structure, Optical Properties, and Electrical Conductivity of a Narrow Bandgap p-Type Semiconducting Polymer

Sarah M. West, Duyen K. Tran, Werner Kaminsky, and Samson A. Jenekhe*

Cite This: *Macromolecules* 2024, 57, 8176−8186 Read Online

ABSTRACT: We report herein the synthesis, electronic structure, experimental and density functional theory (DFT) calculated optical properties, and electrical conductivity of a new π-conjugated ladder polymer, ladder poly(thienobenzothiazine) (LTBT), and its model compound, thienobis(benzothiazine) (TBBT). The synthesis of LTBT in a mixed polyphosphoric acid/sulfolane solvent system gave an intrinsic viscosity of 2.0 dL/g at 30 °C in methanesulfonic acid, and the polymer could form large-area freestanding films. Single-crystal X-ray structure of TBBT showed that it crystallizes in an orthorhombic structure with a coplanar thienobenzothiazine ladder backbone, which is in agreement with the DFT calculated structure. The electrochemically derived HOMO and LUMO energy levels of −5.17 eV and −3.75 eV of LTBT thin films revealed the p-type semiconducting nature of the conjugated ladder polymer. We thus p-doped LTBT thin films with FeCl$_3$, leading to an average electrical conductivity of 0.3 S/cm. These results demonstrate the potential of the new ladder polymer LTBT in organic electronics while providing valuable insights into the structure−property relationships of semiconducting ladder polymers.

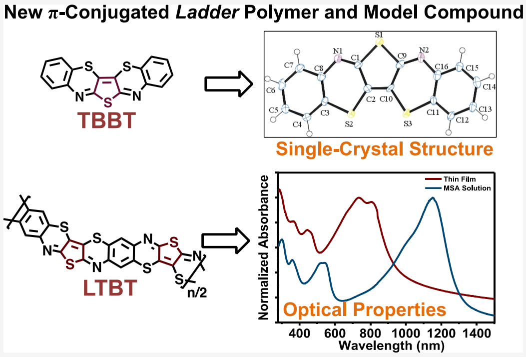

INTRODUCTION

π-Conjugated ladder polymers (CLPs), which are composed of conjugated double-stranded or all-polycyclic architectures, are currently of broad interest for applications in electronics and optoelectronics,[1−18] including thin-film transistors,[6,7] organic photovoltaics,[8,9] organic electrochemical transistors,[10−13] organic thermoelectrics,[14−16] battery electrodes,[19,20] lasers,[21] and polariton transistors.[22] Both n-type and p-type semiconducting CLPs are essential for most of these applications. Recently, conjugated ladder poly(pyrrolobenzothiazine)s (LPBTs) were shown to be a promising class of p-type semiconducting polymers by our group[23] and others.[14,24,25] Toward investigation and understanding of the structure−property relationships in CLPs, the ladder *benzothiazine* backbone[23,24,26,27] offers attractive opportunities in part because in addition to the possibility of side-chain engineering,[23,28] chalcogen substitution is a possibility.

Among heteroatoms found in the structures of π-conjugated polymers, sulfur and thus conjugated polymers based on thiophene building blocks have been the most successful in part because of their ambient chemical and photochemical stability. Thus, the success of thiophene semiconductors originates from the unique properties of the sulfur heteroatom. The sulfur atom in thiophene fosters strong electronic coupling though noncovalent interactions such as π−π, S−H, and S−N in the solid state which can lead to planar geometries.[29−32] Moreover, the larger atomic radius of the sulfur atom and aromaticity of the thiophene ring leads to improved orbital overlap between the highest-occupied molecular orbital (HOMO) energy level of the adjacent atoms in the solid state, which can lower the HOMO energy level of the polymer.[33] An example of the previously reported ladder poly(pyrrolobenzothiazine) (LPBT)[14,23] and its model compound PBBTZ[26,27] are shown in Chart 1a. We have previously showed that the LPBT has a donor−acceptor architecture and thus has strong intramolecular charge transfer (ICT) character in thin films and protic acid solutions. Moreover, previous reports of LPBTs model compound, PBBTZ, (Chart 1a) demonstrated its high polycrystalline[26] and single-crystal[27] field-effect hole mobilities of 0.34 and 3.6 cm^2/(V s), which demonstrate its utility as a p-type semiconductor. Compared to the pyrrole-based LPBT, we expect that substitution of thiophene into the benzothiazine ladder backbone will significantly narrow the optical bandgap and improve the protonation-enhanced ICT interactions in the near-infrared (NIR) region. Such features will make the new ladder polymer an excellent candidate for applications in next generation

Received: April 10, 2024
Revised: July 5, 2024
Accepted: July 25, 2024
Published: August 7, 2024

https://doi.org/10.1021/acs.macromol.4c00817
Macromolecules 2024, 57, 8176−8186

Chart 1. (a) Molecular Structures of Model Compound PBBTZ and p-Type Conjugated Ladder Polymer LPBT and (b) Molecular Structures of Model Compound TBBT and Ladder Polymer LTBT Synthesized in This Study

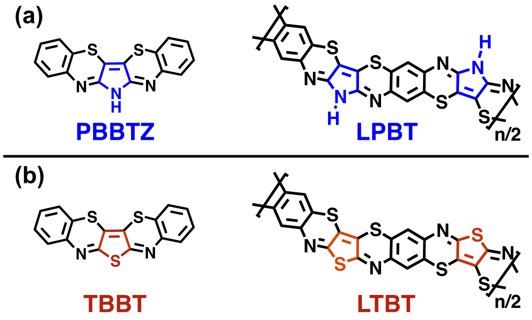

optoelectronic devices such as organic solar cells[34−40] and photodetectors.[39,41−43]

Here, we report the synthesis of a new thiophene-based π-conjugated ladder polymer, ladder poly(thieno[3,2-b:4,5-b']-benzothiazine) (LTBT), and its model compound thieno[3,2-b:4,5-b']bis[1,4]benzothiazine (TBBT) (Chart 1b). We also report detailed investigations of the molecular structure, electronic structure, optical properties, and electrical conductivity of p-doped LTBT. The new ladder polymer LTBT was synthesized by using a unique solvent system to do the polymerization that resulted in excellent film-forming properties as evidenced by large-area freestanding films of LTBT, which were used to characterize the molecular structure by Fourier-transform infrared (FTIR) and Raman spectroscopies. The highly crystalline nature of TBBT enabled solution phase growth of single crystals for X-ray crystal structure determination, which verified the molecular structures of TBBT and LTBT. We found that LTBT has a donor−acceptor structure with respect to the thiophene-benzothiazine backbone, enabling enhanced intramolecular charge transfer (ICT) and a narrow thin-film optical bandgap of 1.28 eV. We measured the electrical conductivity of LTBT doped with $FeCl_3$ to be 0.3 S/cm.

■ EXPERIMENTAL METHODS

Materials and Methods. 2,5-Diamino-1,4-benzenedithiol HCl (97%) was purchased from Ambeed and recrystallized in 20% HCl before use. Perbromothiophene (98%) was purchased from Ambeed and used as received. Polyphosphoric acid (PPA, 84% P_2O_5), sulfolane, methanesulfonic acid (MSA) (>99%), trifluoroacetic acid (TFA), triflic acid, fuming nitric acid (red, 90% > HNO_3), dichloromethane (DCM), acetone, dimethylformamide (DMF), deuterated dimethyl sulfoxide (DMSO-d6), deuterated TFA (TFA-d), $FeCl_3$, and 2-aminobenzenethiol were purchased from Sigma-Aldrich and used as received. Methanol, acetonitrile, and acetic acid were purchased from Fisher Scientific and used as received. All reactions were performed under inert atmosphere unless otherwise stated.

The intrinsic viscosity [η] of LTBT was measured in the MSA solution in an Ubbelohde viscometer suspended in a water bath at 30.0 °C. The concentrations of the polymer solution was chosen such that the elution time of the polymer solution was 1.1−1.8 times that of the pure solvent.

Thermogravimetric analysis (TGA) was conducted on a TA Instrument model Q50 TGA. A heating rate of 10 °C/min under a flow of N_2 was used with runs conducted from room temperature to 880 °C. Differential scanning calorimetry (DSC) analysis was performed on a TA Discovery DSC 500 under N_2 by scanning from −10 to 400 °C at a heating rate and cooling rate of 10 °C/min. Optical absorption spectra were measured on a PerkinElmer model Lambda 900 UV−vis/near-IR spectrophotometer. Solution absorption spectra were obtained from dilute solutions (10^{-5} M) in MSA and triflic acid. The ^1H and ^{13}C NMR spectra were recorded on a Bruker AV500 (at 500 MHz) using deuterated DMSO or TFA as the solvent.

Cyclic voltammetry (CV) experiments were performed on an EG&G Princeton Applied Research potentiostat/galvanostat (model 273A). A three-electrode cell was used, using platinum wires as the counter electrodes and the polymer coated onto a platinum wire from MSA solution as the working electrodes. Solution phase cyclic voltammetry was performed at a concentration of 3 mg/mL. The reference electrode was $Ag/AgNO_3$ in acetonitrile. The acidic solvents in thin films were removed by dipping the substrates in isopropanol (IPA) overnight and subsequently dried in a vacuum oven at 60 °C. The supporting electrolyte solution consists of 0.1 M tetrabutylammonium hexafluorophosphate (Bu_4NPF_6) in anhydrous acetonitrile. The electrolyte was purged with nitrogen for 15 min prior to the scans to ensure inert and anhydrous conditions. The reduction and oxidation potentials were referenced to the Fc/Fc^+ couple by using ferrocene as an internal standard.[44,45] LUMO energy levels were estimated using ferrocene value of −4.8 eV with respect to vacuum level. The LUMO and HOMO levels were determined by using the equations $E_{LUMO} = -(eE_{red}^{onset} + 4.8)$ and $E_{HOMO} = -(eE_{ox}^{onset} + 4.8)$.

Fourier-transform infrared spectroscopy (FTIR) experiments were performed on a PerkinElmer Frontier spectrometer using freestanding films of LTBT and needles of TBBT. The resolution was set at 1 cm^{-1} and a set of 16 scans was averaged. Raman spectroscopy of the freestanding film was carried out on a Thermo Scientific DXR2 Raman microscope. A 532 nm laser with a power of 5 mW was focused on a sample through a 10x objective lens.

Gas-phase density functional theory (DFT) and time-dependent density functional theory (TD-DFT) calculations were performed using the Gaussian 16 suite of programs[46] at the ωB97XD/631-G(d,p) level of theory on the representative oligomers comprising three repeat units. Vertical electronic transitions were calculated for 12 excited states.

Synthesis of 3,4-Dibromothiophene-2,5-dione (DBTD). Fuming nitric acid (35 mL) was added to a reaction vessel and chilled to 0 °C. Then, a mixture of perbromothiophene (5.0 g, 12.5 mmol) in DCM (13.5 mL) was added over 20 min. The reaction mixture was then stirred for 1 h at 0 °C, poured into ice water, extracted with DCM, and washed with water. The solvent was removed on a rotary evaporator and the crude solid obtained was dried at 50 °C in a vacuum oven. The final product was purified using vacuum sublimation at 100 °C where a yellow, crystalline solid was collected (yield 2.5 g, 74%). ^1H NMR (500 MHz, DMSO-d6, δ): no peaks observed. ^{13}C NMR (500 MHz, DMSO-d6, δ): 183.38, 141.03 Anal. Calcd for $C_4Br_2O_2S$ (%): C, 17.67; H, 0.00; O, 11.77; found (%): C, 17.83; H, 0.0; O, 12.51.

Synthesis of 6*H*-Thieno[3,2-*b*:4,5-*b*]bis[1,4]benzothiazine (TBBT). Glacial acetic acid (24 mL) was added to a reaction vessel equipped with a reflux condenser and purged with nitrogen for 15 min. 2-Aminothiophenol (1.00 g, 7.99 mmol) and 3,4-dibromothiophene-2,5-dione (1.09 g, 4.00 mmol) were added, and the mixture was refluxed for 6 h. The reaction mixture was then cooled to room temperature, filtered, and washed with methanol and acetone. The crude solid was then recrystallized in DMF to give red needles (yield, 0.830 g, 64%). ^1H NMR (500 MHz, TFA-d, δ): 7.68 (d, *J* = 6.4 Hz, 2H), 7.56 (m, 6H). Anal. Calcd for $C_{16}H_8N_2S_3$ (%): C, 59.23; H, 2.49; N, 8.63; found (%): C, 59.31; H, 2.16; N, 8.63.

Synthesis of Ladder Poly(thienobenzothiazine) (LTBT). PPA (16.78 g) was added to a reaction flask equipped with a mechanical stirrer and purged with nitrogen at 150 °C overnight. The PPA was cooled to room temperature and 2,5-diamino-1,4-benzenedithiol HCl (1.78 g, 7.17 mmol) was added. Dehydrochlorination was conducted at room temperature for 24 h followed by 70 °C for 24 h. Then, 3,4-dibromothiophene-2,5-dione (1.95 g, 7.17 mmol) dissolved in deoxygenated sulfolane (16.78 g) was added. The polymerization mixture was stirred at 80 °C overnight followed by an incremental

Scheme 1. Synthesis of TBBT and LTBT[a]

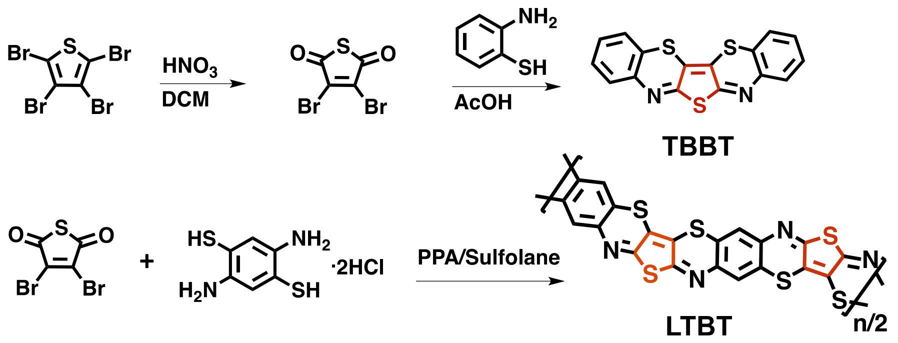

[a]HNO_3 = fuming nitric acid, DCM = dichloromethane, AcOH = acetic acid, PPA = polyphosphoric acid (84% free P_2O_5), and PPA/sulfolane 1:1 (w/w).

temperature increase to 150 °C over 8 h. The temperature of the polymerization mixture was increased to 180 °C over 4 h and was stirred for 40 h. The polymer mixture (dope) was cooled to room temperature, quenched with methanol, and purified under Soxhlet extraction with water for 24 h followed by methanol for 24 h. The crude product was dried and further purified by reprecipitation from MSA solution into methanol (yield 1.67 g, 95%). Intrinsic viscosity ($[\eta]$): 2.0 dL/g (30.0 °C, MSA) Anal. Calcd for $C_{10}H_2N_2S_3$ (%): C, 48.76; H, 0.82; N, 11.37; S, 39.05; found (%): C, 48.48; H, 1.28; N, 11.18.

Preparation of Thin Film, Doping Method, and Characterization of Electrical Conductivity. Solutions of LTBT in methanesulfonic acid (MSA) at 15 mg/mL were stirred at elevated temperature (>140 °C) for at least a day to ensure solubilization of the polymer. The polymer solution in MSA was filtered through 1 μm pore size grade GF/B Glass Microfiber Filters (Whatman GF/B) before use. The filtered polymer solution was then spin-coated onto clean glass substrates (sonicated in acetone, DI water, and isopropanol) at 5000 rpm for 30 s followed by immediate immersion in isopropanol (IPA) for deprotonation. The pH of the deprotonation solvent (IPA) was checked to ensure complete acid removal. The neutral polymer films were dried in a vacuum oven at 60 °C overnight. The measured film thickness by using a profilometer was 94 ± 5 nm.

The undoped neutral polymer films were then moved into a nitrogen-filled glovebox for doping study. A stock solution of 100 mM $FeCl_3$ in anhydrous acetonitrile was made, stored in the glovebox, and diluted to the desired concentration immediately before use. 200 μL of dopant solution (20 mM $FeCl_3$ in acetonitrile) was deposited onto the polymer film (1.5×1.5 cm^2) followed by a 90 s delay before spinning off the excess solution at 7000 rpm for 10 s. The doped polymer films were subjected to thermal annealing at different temperatures. The doped films were brought to ambient atmosphere for further characterizations.

Electrical conductivity (σ_{dc}) of doped LTBT films were measured by a colinear four-point probe controlled by a Keithley 2400 sourcemeter unit. For consistency, a 60-s delay between source and measurements was applied due to the rapid dedoping of the polymer films in ambient environment. The σ_{dc} value was calculated as follows:

$$\sigma_{dc} = \frac{\pi}{\ln(2)} \frac{1}{R \times t}$$

where σ_{dc} is the room-temperature dc-electrical conductivity (S/cm), R is the measured resistance (Ω), and t is the film thickness (cm).

RESULTS AND DISCISSION

Synthesis and Characterization of LTBT and TBBT. The synthetic routes to the model compound TBBT and the target ladder polymer LTBT are shown in Scheme 1 and the detailed synthetic procedures are described in the Experimental Methods section. The 2,5-diamino-1,4-benzenedithiol HCl monomer was purchased with 97% purity and purified according to the published procedure before use.[47] The 3,4-dibromothiophene-2,5-dione (DBTD) monomer was synthesized according to a modified procedure[48] where the perbromothiophene starting material is subjected to oxidation with fuming red nitric acid. The 2,5-aromatic positions are the most reactive toward oxidation and therefore no side products were isolated. Purification of DBTD by vacuum sublimation at 100 °C produced pure yellow crystals in 74% yield that were characterized by ^{1}H NMR (Figure S1), ^{13}C NMR (Figure S2), Fourier-transform infrared (FTIR) spectroscopy (Figure S3), and elemental analysis (Experimental Methods). The model compound for the conjugated ladder polymer, 6H-thieno[3,2-b:4,5-b]bis[1,4]benzothiazine (TBBT), was prepared by condensation of DBTD and 2-aminothiophenol in refluxing acetic acid (Scheme 1). The crude product was recrystallized from N,N-dimethylformamide (DMF), which gave red needles in 64% yield (Figure S4a). TBBT is completely soluble in trifluoroacetic acid (TFA) and methanesulfonic acid (MSA) at room temperature and partially soluble in polar aprotic solvents such as DMF and dimethyl sulfoxide (DMSO). Solutions of TBBT form thin films when spin-coated from TFA onto glass substrates. However, the thin films became highly opaque when submerged in methanol or water to remove the acidic solvent, which is indicative of its highly crystalline nature. The molecular structure of TBBT was characterized by ^{1}H NMR (Figure S4b) FTIR spectroscopy (Figure S5), and single-crystal structure discussed below.

The conjugated ladder polymer, poly(thienobenzothiazine) (LTBT), was prepared by the polycondensation of 2,5-diamino-1,4-benzenedithiol HCl monomer and DBTD monomer in a solvent mixture of polyphosphoric acid (PPA) and sulfolane. Sulfolane was chosen as the cosolvent for several reasons: (1) our previous work on the synthesis of pyrrolobenzothiazine ladder polymers showed that the 2,3-dibromomalemide monomers had limited solubility in pure acid solvents,[23] (2) the DBTD monomer has excellent solubility in sulfolane, and (3) PPA and sulfolane are miscible and stable at high temperatures (>180 °C).[47] Sulfolane and PPA were used in a 1:1 w/w ratio whereby DBTD was dissolved in sulfolane prior to addition to the dehydrochlorinated 2,5-diamino-1,4-benzenedithiol in PPA. An immediate color change from pale yellow to red was seen, indicating good reactivity of the monomers in the PPA/sulfolane solvent system. No sublimation or evaporation of either of the monomers was observed, and a very high polymer yield of 95% indicates excellent incorporation of the monomers into the polymer backbone. We point out that the high yields and straightforward syntheses of both the DBTD monomer, which is synthesized from a commercially available precursor in one step, and the LTBT polymer, which is made in a metal-free single-step polymerization, indicate that they are excellent candidates for large-scale commercialization applications. We note that the polymerization time was limited to 40 h at 180 °C to ensure the solubility of the polymer in MSA; a higher molecular weight LTBT polymer that was originally synthesized by using a 72 h polymerization time was completely insoluble in MSA.

LTBT was isolated as a brown solid and forms purple-red solutions in MSA. The intrinsic viscosity ([η]) was measured to be 2.0 dL/g at 30.0 °C in MSA. Even with [η] of only 2.0 dL/g, the MSA solutions required high temperatures (∼140 °C for 24 h) to ensure complete solubilization at concentrations of 7 mg/mL or higher. Solutions of LTBT in MSA can be spin-coated into thin films or drop cast into freestanding films (Figure 1a). The detailed fabrication procedures to form the thin films and freestanding films are described in the Supporting Information. The freestanding films were used to confirm the molecular structure by performing Fourier-transform infrared (FTIR) and Raman spectroscopies on the freestanding films. The facile fabrication of large-area freestanding films from MSA solutions shows potential for large-area electronic devices to be developed from this π-conjugated polymer.

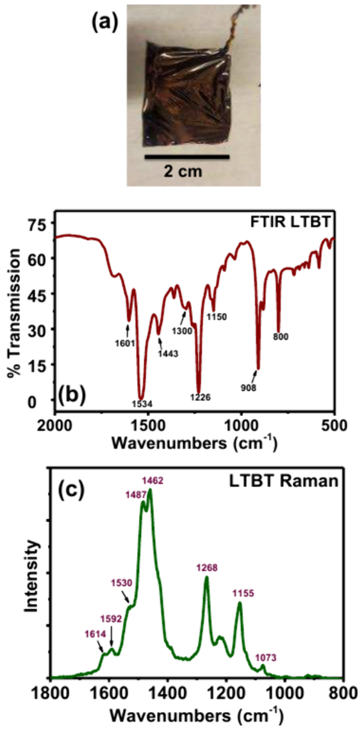

Figure 1. (a) LTBT freestanding film with an area of about 2 × 2 cm^2. (b) Fourier-transform infrared (FTIR) spectrum of the LTBT freestanding film. (c) Raman spectrum of the LTBT freestanding film taken with an excitation laser of 532 nm.

The FTIR and Raman spectra of the LTBT freestanding film (Figure 1) and the FTIR spectrum of the TBBT needles (Figure S5) were collected in ambient atmosphere and the peak positions assigned to the vibrational modes are listed in Tables S1 and S2. The FTIR spectrum of LTBT in Figure 1b shows prominent ν(C=C) stretching modes at 1601 cm^{-1}, and at 1589 and 1564 cm^{-1} for TBBT (Figure S5). Aromatic imine ν(C=N) stretches are seen at 1534 cm^{-1} for LTBT (Figure 1b), and 1539 cm^{-1} for TBBT (Figure S5). At lower wavenumbers, single bond carbon−nitrogen ν(C−N) stretches and carbon−sulfur stretches ν(C−S) can be found at 1226 and 1150 cm^{-1} for LTBT (Figure 1b), and 1238 and 1150 cm^{-1} for TBBT, respectively (Figure S5). The Raman spectra of LTBT in Figure 1c show similar features as the FTIR. The carbon−carbon ν(C=C/C−C) stretch (known as the Я band or "effective coordinate")[49−52] is observed at 1462 cm^{-1} (Figure 1c). Carbon−nitrogen imine ν(C=N) stretches are seen at 1592 and 1530 cm^{-1}, (Figure 1c), and mixed aromatic thiophene/benzene vibrations can be assigned to the high intensity peak at 1487 cm^{-1}. Mixed aromatic intraring modes are seen at 1268 and 1155 cm^{-1}, and the carbon−sulfur stretches ν(C−S) present as a small peak at 1073 cm^{-1} (Figure 1c). The observed FTIR and Raman data collectively provide strong evidence for the backbone fusion and molecular structures of the polymer LTBT and the model compound TBBT.

The thermal stabilities of LTBT and TBBT were probed using thermal gravimetric analysis (TGA) and differential scanning calorimetry (DSC), and the thermograms are shown in Figure S6. Both TBBT and LTBT have high thermal stability, showing 5% weight losses at 324 and 538 °C, respectively, which is indicative of their fused backbone architecture. Additionally, no phase transitions are seen between 0 °C - 300 °C for TBBT, or between 0 °C - 400 °C for LTBT, which agree with other literature reports of conjugated ladder polymers having glass transition temperatures (T_g) over 400 °C.[53]

X-ray Crystal Structure of TBBT. Single crystals of TBBT suitable for X-ray structural determinations were grown via diffusion of ethanol into dilute (∼1 mg/mL) DMF solutions of TBBT and the experimental details for X-ray crystallography and a table of crystallographic data and atomic coordinates are given in the Supporting Information (Tables S3 and S4). Single-crystal X-ray diffraction analysis of TBBT (Figure 2) show that the molecules are aligned in an orthorhombic unit

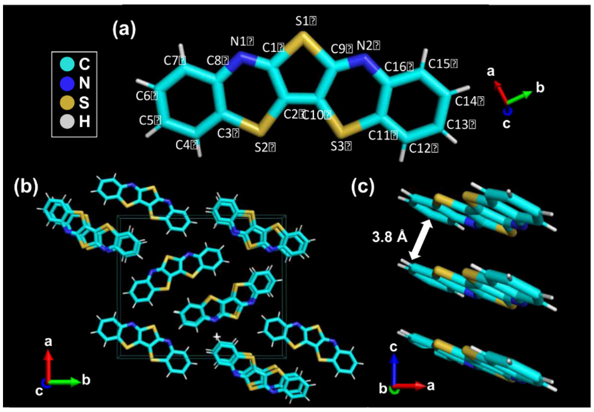

Figure 2. (a) Skeletal structure with atoms placed at the center of the thermal ellipsoids that were calculated at the 50% probability level with atom numbering scheme. (b) Organization of the molecules in a single unit cell. (c) Packing of the molecules along the *c*-axis with an intermolecular distance of 3.8 Å.

cell with a = 17.198(9) Å, b = 20.222(12) Å, c = 3.782(2) Å. The crystals of TBBT have a planar geometry across the central thiophene and benzothiazine moieties (Figure 2a) and form a face-to-face $\pi-\pi$ stacking motif with minimal geometric displacement between neighbors in the $\pi-\pi$ stacking direction (Figure 2b-c). The vertical distance between TBBT molecules is 3.80 Å (Figure 2c). We note that the measured $\pi-\pi$ stacking distance of TBBT is 0.40 Å greater than that reported for the pyrrole-based small molecule PBBTZ (3.40 Å),[26] which is likely due to Pauli repulsion between adjacent sulfur atoms in the TBBT molecules.[31,32] The van der Waals radii of two sulfur atoms is 3.60 Å,[54] which is the theoretical minimum distance between two π-stacked TBBT molecules. The single-crystal structural data of TBBT demonstrates the crystalline nature of the thienobenzothiazine moiety and confirms the molecular structures of the condensation and polycondensation products.

Electronic Structure of LTBT and TBBT. We performed density functional theory (DFT) and time-dependent density functional theory (TD-DFT) calculations at the ωB97XD/6-31G(d,p) level of theory to further our understanding of the ground state and excited state molecular geometry and frontier molecular orbital distributions of LTBT and TBBT. The optimized ground state geometry of LTBT is completely planar (Figure 3a) with HOMO and LUMO molecular orbitals delocalized across the backbone. In order to gain insight into the effects of protonation, calculations were also performed on imine-protonated oligomers bearing a +1 charge (Figure 3b). We note that it is energetically favorable to protonate imine nitrogens over sulfur moieties.[55] The ground state geometry of LTBT remains planar upon protonation (Figure 3b), possibly due to the S···H noncovalent interaction created upon protonation. The calculated distance between the imine hydrogen and thiophene sulfur is 2.83 Å, which is less than the sum of their van der Waals radii (S+H = 2.89 Å),[54] which means that S···H interaction likely contributes to the observed planarity of the protonated polymer chain. Inducing noncovalent interactions is a widely exploited strategy used to reduced the conformational distortions in many π-conjugated polymers, such as those containing diketopyrroles,[56,57] functionalized thiophenes,[58] and pyrazines. The pictoral representation of the HOMO and LUMO orbital distributions of the protonated oligomer bearing a +1 charge is shown in Figure 3b; clearly, protonation induces strong spatial localization of the molecular orbitals, suggesting that LTBT will have strong protonation-enhanced intramolecular charge transfer (ICT) character in acidic solvents.[59] TBBT also has a planar ground-state geometry and delocalized HOMO and LUMO orbital distributions as shown in Figure S7.

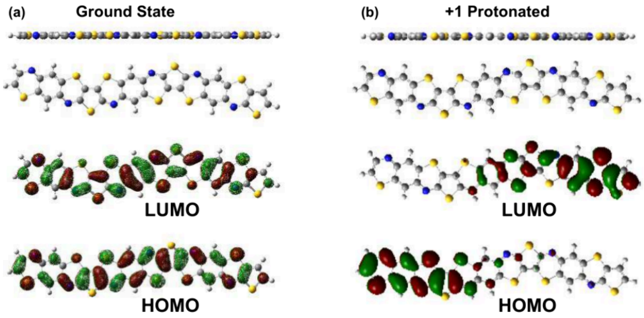

Figure 3. DFT calculated optimized ground-state geometry and the pictoral representation of the frontier molecular orbital distributions of (a) the neutral oligomer and (b) the protonated (+1) oligomer. Calculations performed at the ωB97XD/6-31G(d,p) level of theory.

The TD-DFT calculated excited-state geometry, optical absorption spectrum, and the corresponding pictorial representations of the molecular orbitals associated with the lowest-energy transition for LTBT is shown in Figure S8. The excited-state geometry is coplanar with delocalized HOMO and LUMO energy levels distributed across the ladder polymer backbone, and the $\pi-\pi^*$ transition is centered at 1170 nm, which indicates this polymer may have a narrow experimental optical bandgap.

The reorganizational energy (λ) of LTBT was calculated from the sum of relaxation energies in the neutral and cationic state to gain insight into the energy associated with geometry changes upon charge injection.[60,61] Figure S9 shows the cationic geometry and the polaron orbital distribution of the oligomer. A fairly large reorganizational energy of 1.39 eV was calculated for LTBT, which could suggest that LTBT undergoes geometry changes upon charge injection and may not have a rigid-rod chain topology like BBL.[7,62,63] Note that the calculated λ decrease with polymer chain length and thus more accurate reorganizational energy calculations would require more than 12 repeat units.[61]

We further investigated the electronic structures of LTBT and TBBT by using cyclic voltammetry (CV) measurements. The HOMO and LUMO energy levels of TBBT and LTBT are summarized in Table 1, and the oxidation waves of LTBT thin films coated on platinum wires and of TBBT needles dissolved in acetonitrile at 10^{-5} M in 0.1 M tetrabutylammonium hexafluorophosphate (Bu_4NPF_6) with $Ag/AgNO_3$ as the reference electrode are shown in Figure 4a-b. The reduction waves are shown in Figure S10. LTBT shows two quasi-reversible oxidation waves at 1.29 and 1.85 V (Figure 4a), and one nonreversible reduction wave (Figure S10a) at −0.87 V. The onset oxidation potential of 0.90 V and onset reduction potential of −0.59 V were used to estimate the HOMO and LUMO energy levels of −5.17 eV and −3.75 eV, respectively (Table 1), which are 0.21 and 0.48 eV deeper than that of HOMO and LUMO energy levels that we measured for LPBT.[23] The model compound TBBT shows two nonreversible oxidation waves, which are centered at 1.45 and 1.85 V (Figure 4b), and one nonreversible reduction wave at −1.22 V (Figure S10b). The TBBT onset oxidation and reduction potentials of 1.48 V and −0.66 V, respectively, were used to measure the HOMO/LUMO energy levels of −6.37 eV/−3.59 eV, which are lowered compared to the pyrrole-based compound, PBBTZ (HOMO = −5.44 eV, LUMO =

Table 1. Electronic Structure Parameters and Optical Properties of LTBT and TBBT

	HOMO (eV)	LUMO (eV)	$E_g^{\text{elec.}}$ (eV)	$\lambda_{\max}{}^{a}$ (nm)	$\varepsilon_{\max}{}^{a}$ (M^{-1} cm^{-1})	$\lambda_{\max}{}^{b}$ (nm)	$\alpha_{\max}{}^{b}$ (cm^{-1})	$E_g^{\text{opt.}b}$ (eV)	$\lambda_{\max}{}^{c}$ (nm)
LTBT	−5.17	−3.75	1.42	1151	2.4 x10^4	825	9.9 x10^4	1.28	1192
TBBT	−6.37	−3.59	2.78	693	1.9 x10^4	525	4.4 x10^4	2.05	—

[a] Solution in MSA. [b] Thin film on glass. [c] Solution in TfOH.

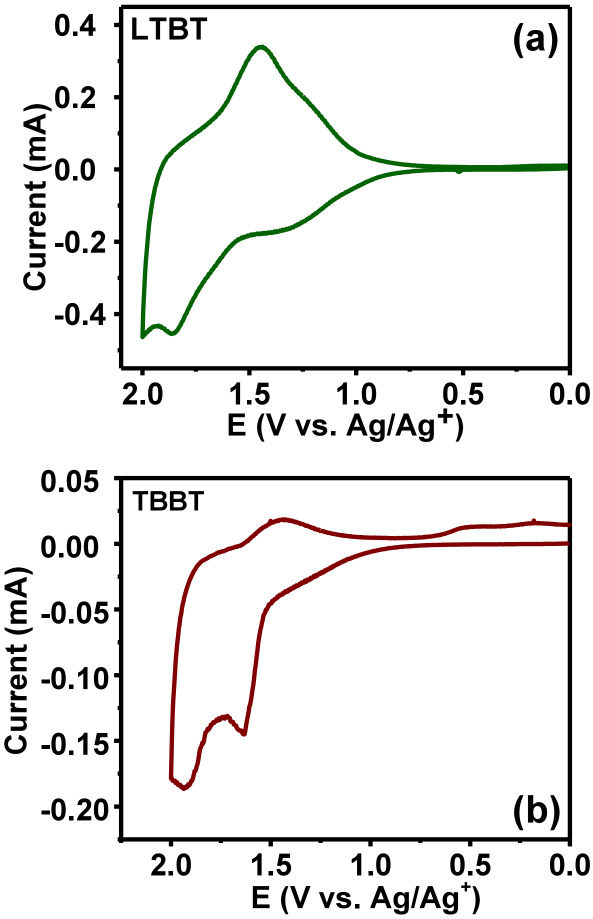

Figure 4. Cyclic voltammograms measured in 0.1 M Bu_4NPF_6 electrolyte solution using Ag/$AgNO_3$ as the reference electrode of the oxidation processes of (a) LTBT thin films coated on platinum wires and (b) TBBT needles in solution. The scan rate was 100 mV/s.

−3.03 eV).[26] The electrochemical bandgaps ($E_g^{\text{elec.}}$) are 1.42 and 2.78 eV for LTBT and TBBT, respectively (Table 1).

Optical Properties of LTBT and TBBT. The optical absorption spectra of LTBT and TBBT in MSA solution and in thin film are shown in Figures 5 and the lowest energy peak positions (λ_{max}), optical band gap ($E_g^{\text{opt.}}$), molar absorptivity (ε_{max}), and absorption coefficient (α_{max}) are summarized in Table 1. The MSA-solution optical absorption spectrum of TBBT (Figure 5a) shows peaks in the 300 nm −700 nm region with the $\pi-\pi^*$ transition assigned to the peak at 455 nm (ε_{max} = 1.5 × 10^4 M^{-1} cm^{-1}) and a lowest energy peak at 693 nm (ε_{max} = 1.9 × 10^4 M^{-1} cm^{-1}) which can be attributed to protonation-enhanced intramolecular charge transfer (ICT), a phenomenon which is seen in many imine-bearing π-conjugated systems.[64] For LTBT, the MSA-solution absorption spectrum (Figure 5a) shows three high-energy bands at 302 nm (ε_{max} = 1.6 × 10^4 M^{-1} cm^{-1}), 362 nm (ε_{max} = 1.2 × 10^4 M^{-1} cm^{-1}), and 532 nm (ε_{max} = 1.2 × 10^4 M^{-1} cm^{-1}), of which the latter can be assigned to the $\pi-\pi^*$ transition. The intense lowest-energy band at 1151 nm (ε_{max} = 2.4 × 10^4 M^{-1} cm^{-1}) originates from protonation-enhanced intramolecular charge transfer. The effects of protonation on the ICT band are corroborated by the previously discussed DFT calculations (Figure 3b) whereby protonation induces spatial localization of the HOMO and LUMO molecular orbitals that correspond to the observed ICT character in MSA solution (Figure 3b).

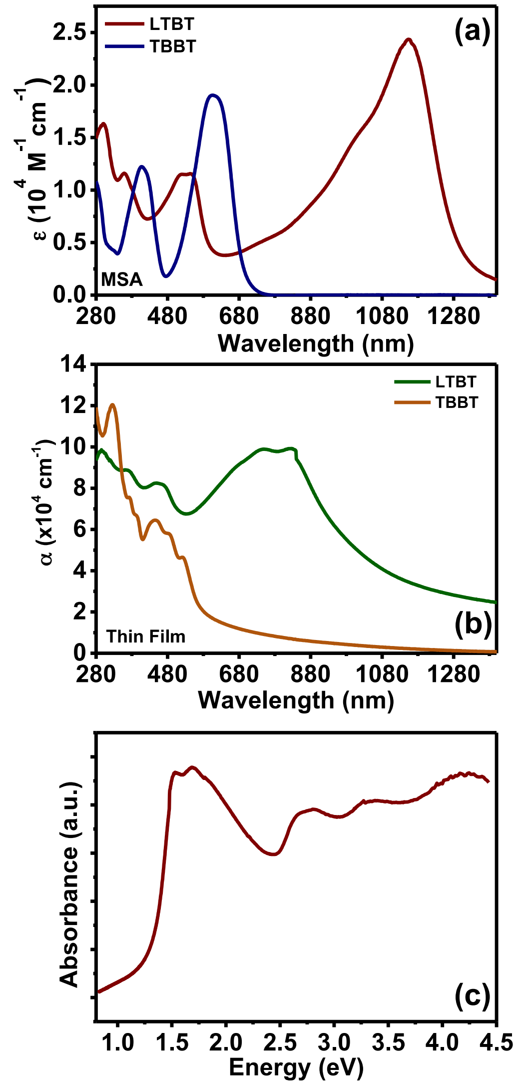

Figure 5. Optical absorption spectra of TBBT and LTBT in (a) dilute MSA solution (10^{-5} M) and (b) as thin films on glass substrates. (c) The thin film absorption spectrum of LTBT plotted vs energy (eV) to determine the optical bandgap.

The thin-film absorption spectrum of TBBT (Figure 5b) has multiple peaks in the 300−525 nm region, and the lowest-energy peak ($\pi-\pi^*$ transition) is centered at 525 nm (α_{max} = 4.4 x10^4 cm^{-1}). The optical bandgap calculated from the onset of absorption in Figure S11 is 2.05 eV, which is 0.73 eV smaller than the electrochemical bandgap ($E_g^{\text{elec.}}$) of 2.78 eV, which suggests that TBBT may have a large effective exciton binding energy (E_b).[65−67] Compared to the thin film absorption spectra, in MSA solutions the lowest energy peak is red-shifted by 168 nm (Table 1), which demonstrates that the ICT character of TBBT, like the polymer LTBT, is similarly enhanced by protonation.

The thin-film absorption spectrum of LTBT (Figure 5b) shows peaks between 300 nm −900 nm with the $\pi-\pi^*$ peak centered at 825 nm (α_{max}= 9.9 x10^4 cm^{-1}). The optical bandgap ($E_g^{\text{opt.}}$) measured from the onset of the thin film absorption is 1.28 eV (Figure 5c), which is 0.14 eV smaller than the $E_g^{\text{elec.}}$ of 1.42 eV (Table 1), indicating a reduced E_b of 0.14 eV compared to model compound (Table 1). We note that the optical bandgap of LTBT is narrowed by 0.21 eV compared to LPBT,[23] which is explained by the enhanced effective conjugation length of LTBT that originates from the replacement of the pyrrole donor moiety with thiophene. In contrast to the optical absorption spectrum in MSA, the thin film absorption spectrum is markedly different. In particular, the MSA solution absorption spectrum with the lowest-energy absorption peak at 1151 nm is red-shifted by 326 nm from that of the thin film (λ_{max} = 825 nm). The large 326 nm difference in the lowest-energy peak positions confirms protonation enhancement of the ICT character as previously discussed.

To gauge the polymer chain topology in protic acid solutions, variable-temperature optical absorption spectra were collected in both MSA and triflic acid solutions ranging from 20 °C − 100 °C (Figure S12). In the MSA solution absorption spectrum, increasing the temperature results in the ICT band blue shifting from 1151 nm at 20 °C to 1107 nm at 100 °C accompanied by decreasing molar absorptivity and vibronic structures (Figure S12a). In contrast to the MSA solution, the variable-temperature absorption spectrum in triflic acid does not show any changes of the λ_{max} (Figure S12b). The observed thermochromism in MSA solution means that the polymer chain topology is semiflexible when partially protonated in weaker acids like MSA (pK_a ∼ −2).[68] However, when fully protonated in triflic acid (pK_a ∼ −14) the LTBT polymer chain is more rigid. Clearly, LTBT is not a rigid-rod polymer; this is in contrast to the rigid-rod ladder polymer BBL that shows no thermochromism in MSA solutions in the same temperature range.[23] The increased flexibility of the partially protonated LTBT backbone agrees with the results of the previously reported variable-temperature optical absorption spectra of the *pyrrole*-based benzothiazine ladder polymers in which we found that the benzothiazine ladder polymers showed substantial thermochromism in MSA solutions, whereas minimal to no thermochromism was shown in triflic acid solutions in which they are fully protonated.[23] Observed thermochromism can be understood to arise from the polymer chain becoming more disordered (e.g., bent) upon heating, resulting in a decreased π-conjugation length and therefore a blue-shifted λ_{max} relative to the more ordered (i.e., planar) polymer chains at lower temperatures. The thermochromic trends observed in LTBT suggest that substitution of a thiophene moiety in LTBT for the pyrrole moiety in LPBT has minimal effect on the benzothiazine ladder polymer chain rigidity.

Electrical Conductivity of Doped LTBT Thin Films. We used ferric chloride ($FeCl_3$) as a p-type dopant to study the electrical conductivity of doped LTBT thin films, since it has been demonstrated to have a low electron affinity (EA ∼ 5.5 eV)[14] and capable of effectively oxidizing various p-type conjugated polymers.[14,69−74] Detailed doping procedure is described in the Experimental Methods section, wherein solution-sequential processing[75] was used to dope LTBT thin films. This strategy has been showed to be a highly effective technique to produce highly conducting polymer films by means of fine-tuning dopant diffusion into the polymer film without compromising film quality, creating large dopant aggregates, or disrupting the polymer crystal structures.[76−80] In short, the dopant solution (20 mM $FeCl_3$ in acetonitrile) was deposited onto the neat LTBT thin films followed by a 90-s delay before spinning off the excess solution. The doped polymer films were then thermally annealed at various temperatures prior to characterizing the room-temperature dc-electrical conductivity (σ_{dc}) via colinear four-point probe technique in ambient environment. The numerical values of σ_{dc} as a function of annealing temperatures and its room-temperature stability are summarized in Table 2.

Table 2. Dc-Electrical Conductivity (σ_{dc}) of $FeCl_3$-Doped LTBT Thin Films as a Function of Annealing Temperature and Storage Duration

Variable	Condition	$\sigma_{dc,\ average}$ (S/cm)[a]
Annealing Temperature	80 °C − 10 min	$(1.1 \pm 0.3) \times 10^{-1}$
	100 °C − 10 min	(3.3 ± 0.3) x10^{-1}
	120 °C − 10 min	$(2.7 \pm 1.1) \times 10^{-1}$
	140 °C − 10 min	$(1.4 \pm 1.0) \times 10^{-1}$
Stability	Day 0	$(3.3 \pm 0.3) \times 10^{-1}$
	Day 1	$(4.5 \pm 0.8) \times 10^{-2}$
	Day 2	$(1.3 \pm 0.5) \times 10^{-3}$
	Day 3	$(1.1 \pm 0.6) \times 10^{-3}$
	Day 4	$(7.1 \pm 4.4) \times 10^{-4}$

[a] Average values are obtained from three different samples.

Upon the deposition of $FeCl_3$, the initially forest-green colored undoped LTBT films turned brown indicating successful doping reactions and the formation of polaronic charge carriers. However, the brown-colored doped films quickly turned to green-colored films within seconds of exposing them to air indicating rapid dedoping and quenching of polarons/bipolarons due to side reactions with either oxygen or moisture.[81]

Undoped LTBT films were insulating with a very high resistance (≫10^6 Ω). Upon doping with $FeCl_3$ and after annealing at 100 °C for 10 min, LTBT films exhibited an average σ_{dc} of $(3.3 \pm 0.3) \times 10^{-1}$ S/cm (Table 2) with a maximum value of 3.8×10^{-1} S/cm. Higher annealing temperatures resulted in a rapid decrease in electrical conductivity (Figure 6a) suggesting thermal dedoping, which could be attributed to dopant diffusion at higher temperatures.[82,83] We note that the σ_{dc} of doped LTBT films are rather modest compared to state-of-the-art p-type conducting polymers, considering that the thermodynamic requirements

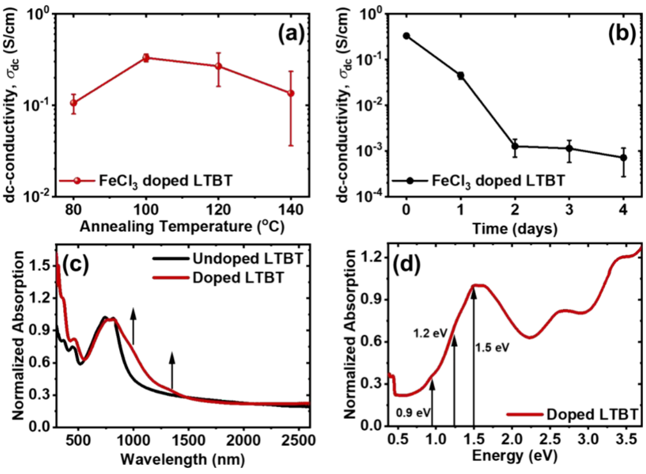

Figure 6. (a) Dc-electrical conductivity (σ_{dc}) of $FeCl_3$ doped LTBT thin films at various annealing temperatures. (b) Stability of electrical conductivity of LTBT doped films in ambient air. (c) Thin film optical absorption spectra of undoped and $FeCl_3$ doped LTBT thin films. (d) Optical absorption spectra of LTBT doped films in energy space.

for efficient doping are sufficiently achieved ($\mathrm{HOMO}_{\mathrm{LTBT}} < \mathrm{LUMO}_{\mathrm{FeCl3}}$). Atomic force microscopy (AFM) imaging showed that the surfaces of LTBT neat films were rather rough with large aggregates (RMS roughness ∼5−7 nm), especially when probed over large dimensions (1−2 μm) (Figure S13). Such suboptimal surface morphology could hinder diffusion of $\mathrm{FeCl_3}$ molecules into the polymer films; thus, limiting the electrical conductivity. Furthermore, the rapid dedoping in ambient conditions partly contributed to the low σ_{dc} of doped LTBT films. As a result of the observed air instability of LTBT doped film, we also monitored the room-temperature electrical conductivity over several days. The σ_{dc} values decreased by over 2 orders of magnitude within the first 2 days before leveling off at around 10^{-3} S/cm. Despite its relatively poor ambient stability, LTBT still showed at least several orders of magnitude enhancement of conductivity upon doping; thus, suggesting its potential for future device applications.

UV−vis-NIR optical absorption spectroscopy was used to further confirm the formation of polaronic species and rationalize the modest electrical conductivity of $\mathrm{FeCl_3}$ doped LTBT films. Upon doping, the vibronic features of the $\pi-\pi^*$ transition band were diminished and accompanied by two new broad absorption bands centered at around 1000 nm (1.2 eV) and 1345 nm (0.9 eV) (Figures 6c and 6d), indicating the generation of polaronic charge carriers. However, the lack of absorption extending to further NIR region (>1500 nm) suggests that charge carriers in $\mathrm{FeCl_3}$ doped LTBT are rather localized,[14] which further explains the observed modest electrical conductivity.

Currently, the prototype n-type ladder polymer BBL is the state-of-the-art π-conjugated polymer used in OECTs,[10,12,13,84] and has shown high electrical conductivities of ∼8.0 S/cm when n-doped with poly(ethylenimine).[85] An n-type derivative of BBL that features a phenazine moiety, BBL-P, has recently shown novel features, including "super-Nernstian" proton-coupled electron transfer reactions.[86,87] There are clearly many advantages of ladder polymers such as LTBT, which include facile, scalable synthesis and processability into high-quality thin films for device applications. In particular, we believe that the narrow bandgap and strong donor−acceptor character of LTBT makes it an attractive p-type semiconducting polymer for solar cell applications.[88−90]

■ CONCLUSIONS

In this study, we report the synthesis and characterization of the electronic structure, optical properties, and electrical conductivity of the new p-type semiconducting ladder polymer, ladder poly(thienobenzothiazine) (LTBT). We also synthesized thienobis(benzothiazine) (TBBT), the model compound of LTBT, and obtained its single-crystal structure which confirmed the molecular structure and planar ladder structure of LTBT. LTBT has excellent film-forming properties as evidenced by the large area freestanding films. A combination of DFT calculations and optical absorption measurements revealed that LTBT has a strong donor−acceptor character that enabled a narrow optical bandgap of 1.28 eV. Moreover, protonation-enhanced intramolecular charge transfer (ICT) character was observed in the infrared region in MSA-solution absorption spectra, evidenced by a 326 nm red shift of the lowest energy peak compared to the thin film absorption spectrum.

The average electrical conductivity was measured to be (3.3 ± 0.3) × 10^{-1} S/cm when LTBT was p-doped with $\mathrm{FeCl_3}$. The modest electrical conductivity of LTBT is attributed to the combination of poor air stability of the doped polymer films and the rough film surface that was seen on AFM imaging. These results demonstrate the potential of the new thiophene-based p-type semiconducting ladder polymer LTBT in organic electronics while providing new insights into the structure−property relationships of semiconducting ladder polymers in general.

■ ASSOCIATED CONTENT

Supporting Information

. The Supporting Information is available free of charge at https://pubs.acs.org/doi/10.1021/acs.macromol.4c00817.

Preparation of freestanding films, experimental details of X-ray crystallography, NMR and FTIR spectra, TGA and DSC traces, DFT results for the geometry and HOMO/LUMO orbitals of TBBT, TD-DFT results and simulated absorbance spectrum, DFT results for cationic geometry and polaron wave function, reduction waves of LTBT and TBBT, thin film absorption spectra plotted vs energy (eV), variable temperature optical absorbance spectra, AFM images, tables of FTIR and Raman stretches, crystallographic data for TBBT, and supporting references (PDF)

Crystallographic information (CIF)

■ AUTHOR INFORMATION

Corresponding Author

Samson A. Jenekhe − *Department of Chemistry, University of Washington, Seattle, Washington 98195-1750, United States; Department of Chemical Engineering, University of Washington, Seattle, Washington 98195-1750, United States*; orcid.org/0000-0002-0898-9541; Email: jenekhe@uw.edu

Authors

Sarah M. West − *Department of Chemistry, University of Washington, Seattle, Washington 98195-1750, United States*
Duyen K. Tran − *Department of Chemical Engineering, University of Washington, Seattle, Washington 98195-1750, United States*; orcid.org/0000-0002-3065-6153
Werner Kaminsky − *Department of Chemistry, University of Washington, Seattle, Washington 98195-1750, United States*

Complete contact information is available at: https://pubs.acs.org/10.1021/acs.macromol.4c00817

Notes

The authors declare no competing financial interest.

■ ACKNOWLEDGMENTS

This work was supported by the National Science Foundation (Grant DMR-2003518). Part of this work was conducted at the Molecular Analysis Facility, a National Nanotechnology Coordinated Infrastructure (NNCI) site at the University of Washington with partial support from the National Science Foundation via Awards NNCI-2025489 and NNCI-1542101. Part of this work was conducted using equipment in the Biomedical Diagnostic Foundry for Translational Research sponsored by the M. J. Murdock Charitable Trust. The DFT calculations were done through the use of advanced computational, storage, and networking infrastructure provided by the Hyak supercomputer system at the University of Washington.

■ REFERENCES

(1) Schlüter, A.-D. Ladder Polymers: The New Generation. *Adv. Mater.* **1991**, *3* (6), 282−291.

(2) Scherf, U.; Müllen, K. The Synthesis of Ladder Polymers. *Adv. Polym. Sci.* **1995**, *123*, 1−40.

(3) Scherf, U. Ladder-Type Materials. *J. Mater. Chem.* **1999**, *9* (9), 1853−1864.

(4) Lee, J.; Kalin, A. J.; Yuan, T.; Al-Hashimi, M.; Fang, L. Fully Conjugated Ladder Polymers. *Chem. Sci.* **2017**, *8* (4), 2503−2521.

(5) Cao, Z.; Leng, M.; Cao, Y.; Gu, X.; Fang, L. How Rigid Are Conjugated Non-Ladder and Ladder Polymers? *J. Polym. Sci.* **2022**, *60* (3), 298.

(6) Babel, A.; Jenekhe, S. A. High Electron Mobility in Ladder Polymer Field-Effect Transistors. *J. Am. Chem. Soc.* **2003**, *125* (45), 13656−13657.

(7) Tran, D. K.; West, S. M.; Guo, J.; Chen, S. E.; Ginger, D. S.; Jenekhe, S. A. Chain Length Dependence of Electron Transport in an N-Type Conjugated Polymer with a Rigid-Rod Chain Topology. *J. Am. Chem. Soc.* **2024**, *146* (2), 1435−1446.

(8) Jenekhe, S. A.; Yi, S. Efficient Photovoltaic Cells from Semiconducting Polymer Heterojunctions. *Appl. Phys. Lett.* **2000**, *77* (17), 2635−2637.

(9) Alam, M. M.; Jenekhe, S. A. Efficient Solar Cells from Layered Nanostructures of Donor and Acceptor Conjugated Polymers. *Chem. Mater.* **2004**, *16* (23), 4647−4656.

(10) Sun, H.; Vagin, M.; Wang, S.; Crispin, X.; Forchheimer, R.; Berggren, M.; Fabiano, S. Complementary Logic Circuits Based on High-Performance n-Type Organic Electrochemical Transistors. *Adv. Mater.* **2018**, *30* (9), 1704916.

(11) Surgailis, J.; Savva, A.; Druet, V.; Paulsen, B. D.; Wu, R.; Hamidi-Sakr, A.; Ohayon, D.; Nikiforidis, G.; Chen, X.; McCulloch, I.; Rivnay, J.; Inal, S. Mixed Conduction in an N-Type Organic Semiconductor in the Absence of Hydrophilic Side-Chains. *Adv. Funct. Mater.* **2021**, *31* (21), 2010165.

(12) Wu, H.-Y.; Yang, C.-Y.; Li, Q.; Kolhe, N. B.; Strakosas, X.; Stoeckel, M.-A.; Wu, Z.; Jin, W.; Savvakis, M.; Kroon, R.; Tu, D.; Woo, H. Y.; Berggren, M.; Jenekhe, S. A.; Fabiano, S. Influence of Molecular Weight on the Organic Electrochemical Transistor Performance of Ladder-Type Conjugated Polymers. *Adv. Mater.* **2022**, *34* (4), 2106235.

(13) Guo, J.; Flagg, L. Q.; Tran, D. K.; Chen, S. E.; Li, R.; Kolhe, N. B.; Giridharagopal, R.; Jenekhe, S. A.; Richter, L. J.; Ginger, D. S. Hydration of a Side-Chain-Free n-Type Semiconducting Ladder Polymer Driven by Electrochemical Doping. *J. Am. Chem. Soc.* **2023**, *145* (3), 1866−1876.

(14) Tam, T. L. D.; Lin, M.; Chien, S. W.; Xu, J. Facile Synthesis of Solubilizing a Group-Free, Solution-Processable p-Type Ladder Conjugated Polymer and Its Thermoelectric Properties. *ACS Macro Lett.* **2022**, *11* (1), 110−115.

(15) Wang, S.; Sun, H.; Ail, U.; Vagin, M.; Persson, P. O. Å.; Andreasen, J. W.; Thiel, W.; Berggren, M.; Crispin, X.; Fazzi, D.; Fabiano, S. Thermoelectric Properties of Solution-Processed n-Doped Ladder-Type Conducting Polymers. *Adv. Mater.* **2016**, *28* (48), 10764−10771.

(16) Tam, T. L. D.; Lin, M.; Handoko, A. D.; Lin, T. T.; Xu, J. High-Performance & Thermally Stable n-Type Polymer Thermoelectrics Based on a Benzyl Viologen Radical Cation-Doped Ladder-Type Conjugated Polymer. *J. Mater. Chem. A* **2021**, *9*, 11787−11793.

(17) Yang, J. S.-J.; Fang, L. Conjugated Ladder Polymers: Advances from Syntheses to Applications. *Chem.* **2024**, *10* (6), 1668−1724.

(18) Leng, M.; Koripally, N.; Huang, J.; Vriza, A.; Lee, K. Y.; Ji, X.; Li, C.; Hays, M.; Tu, Q.; Dunbar, K.; Xu, J.; Ng, T. N.; Fang, L. Synthesis and Exceptional Operational Durability of Polyaniline-Inspired Conductive Ladder Polymers. *Mater. Horiz.* **2023**, *10* (10), 4354−4364.

(19) Ma, T.; Yang, Y.; Johnson, D.; Hansen, K.; Xiang, S.; Thakur, R. M.; Djire, A.; Lutkenhaus, J. L. Understanding the Mechanism of a Conjugated Ladder Polymer as a Stable Anode for Acidic Polymer-Air Batteries. *Joule* **2023**, *7* (10), 2261−2273.

(20) Volkov, A.; Sun, H.; Kroon, R.; Ruoko, T.; Che, C.; Edberg, J.; Muller, C.; Fabiano, S.; Crispin, X. Asymmetric Aqueous Supercapacitor Based on P- and n-Type Conducting Polymers. *ACS Appl. Energy Mater.* **2019**, *2* (8), 5350−5355.

(21) Kallinger, C.; Hilmer, M.; Haugeneder, A.; Perner, M.; Spirkl, W.; Lemmer, U.; Feldmann, J.; Scherf, U.; Müllen, K.; Gombert, A.; Wittwer, V. A Flexible Conjugated Polymer Laser. *Adv. Mater.* **1998**, *10* (12), 920−923.

(22) Zasedatelev, A. V.; Baranikov, A. V.; Urbonas, D.; Scafirimuto, F.; Scherf, U.; Stöferle, T.; Mahrt, R. F.; Lagoudakis, P. G. A Room-Temperature Organic Polariton Transistor. *Nat. Photonics* **2019**, *13* (6), 378−383.

(23) West, S. M.; Tran, D. K.; Guo, J.; Chen, S. E.; Ginger, D. S.; Jenekhe, S. A. P-Type Semiconducting Ladder Poly(Pyrrolobenzothiazine)s: Effects of N-Alkyl Side Chains on the Chain Conformation, Electronic Structure, and Charge Transport Properties. *Macromolecules* **2023**, *56* (24), 10222−10235.

(24) He, Q.; Tam, T. L. D.; Koh, X. Q.; Tham, N. N.; Meng, H.; Huang, W.; Xu, J. P- and N-Dopable Ambipolar Bulk Heterojunction Thermoelectrics Based on Ladder-Type Conjugated Polymers. *J. Mater. Chem. C* **2022**, *11* (1), 204−210.

(25) Wu, H.-Y.; Huang, J.-D.; Jeong, S. Y.; Liu, T.; Wu, Z.; van der Pol, T.; Wang, Q.; Stoeckel, M.-A.; Li, Q.; Fahlman, M.; Tu, D.; Woo, H. Y.; Yang, C.-Y.; Fabiano, S. Stable Organic Electrochemical Neurons Based on P-Type and n-Type Ladder Polymers. *Mater. Horiz.* **2023**, *10*, 4213−4223.

(26) Hong, W.; Wei, Z.; Xi, H.; Xu, W.; Hu, W.; Wang, Q.; Zhu, D. 6H-Pyrrolo[3,2-b:4,5-B′]Bis[1,4]Benzothiazines: Facilely Synthesized Semiconductors for Organic Field-Effect Transistors. *J. Mater. Chem.* **2008**, *18* (40), 4814−4820.

(27) Wei, Z.; Hong, W.; Geng, H.; Wang, C.; Liu, Y.; Li, R.; Xu, W.; Shuai, Z.; Hu, W.; Wang, Q.; Zhu, D. Organic Single Crystal Field-Effect Transistors Based on 6H-Pyrrolo[3,2-b:4,5-B]Bis[1,4]Benzothiazine and Its Derivatives. *Adv. Mater.* **2010**, *22* (22), 2458−2462.

(28) He, Q.; Wang, J.; Dexter Tam, T. L.; Zhang, X.; Jiang, Z.; Chien, S. W.; Tham, N. N.; Koh, X. Q.; Soh, P. X.; Meng, H.; Huang, W.; Xu, J. Thermoelectric Performance Enhancement of P-Type Pyrrolo[3,2-b:4,5-B′]Bis[1,4]Benzothiazine Conjugated Ladder Polymer by Pendant Group Engineering. *ACS Materials Lett.* **2023**, *5* (10), 2829−2835.

(29) Minemawari, H.; Yamada, T.; Matsui, H.; Tsutsumi, J.; Haas, S.; Chiba, R.; Kumai, R.; Hasegawa, T. Inkjet Printing of Single-Crystal Films. *Nature* **2011**, *475* (7356), 364−367.

(30) Izawa, T.; Miyazaki, E.; Takimiya, K. Molecular Ordering of High-Performance Soluble Molecular Semiconductors and Re-Evaluation of Their Field-Effect Transistor Characteristics. *Adv. Mater.* **2008**, *20* (18), 3388−3392.

(31) Liu, B.; Rocca, D.; Yan, H.; Pan, D. Beyond Conformational Control: Effects of Noncovalent Interactions on Molecular Electronic Properties of Conjugated Polymers. *JACS Au* **2021**, *1* (12), 2182−2187.

(32) Huang, H.; Yang, L.; Facchetti, A.; Marks, T. J. Organic and Polymeric Semiconductors Enhanced by Noncovalent Conformational Locks. *Chem. Rev.* **2017**, *117* (15), 10291−10318.

(33) Zhang, W.; Liu, Y.; Yu, G. Heteroatom Substituted Organic/Polymeric Semiconductors and Their Applications in Field-Effect Transistors. *Adv. Mater.* **2014**, *26* (40), 6898−6904.

(34) Meng, L.; Zhang, Y.; Wan, X.; Li, C.; Zhang, X.; Wang, Y.; Ke, X.; Xiao, Z.; Ding, L.; Xia, R.; Yip, H.-L.; Cao, Y.; Chen, Y. Organic and Solution-Processed Tandem Solar Cells with 17.3% Efficiency. *Science* **2018**, *361* (6407), 1094−1098.

(35) Bailey-Salzman, R. F.; Rand, B. P.; Forrest, S. R. Semitransparent Organic Photovoltaic Cells. *Appl. Phys. Lett.* **2006**, *88* (23), 233502.

(36) Zhang, J.; Xu, G.; Tao, F.; Zeng, G.; Zhang, M.; Yang, Y.; Li, Y.; Li, Y. Highly Efficient Semitransparent Organic Solar Cells with Color Rendering Index Approaching 100. *Adv. Mater.* **2019**, *31* (10), 1807159.

(37) Zhu, C.; Huang, H.; Jia, Z.; Cai, F.; Li, J.; Yuan, J.; Meng, L.; Peng, H.; Zhang, Z.; Zou, Y.; Li, Y. Spin-Coated 10.46% and Blade-Coated 9.52% of Ternary Semitransparent Organic Solar Cells with 26.56% Average Visible Transmittance. *J. Sol. Energy* **2020**, *204*, 660−666.

(38) Cheng, P.; Yang, Y. Narrowing the Band Gap: The Key to High-Performance Organic Photovoltaics. *Acc. Chem. Res.* **2020**, *53* (6), 1218−1228.

(39) Ding, L.; Yu, Z.-D.; Wang, X.-Y.; Yao, Z.-F.; Lu, Y.; Yang, C.-Y.; Wang, J.-Y.; Pei, J. Polymer Semiconductors: Synthesis, Processing, and Applications. *Chem. Rev.* **2023**, *123* (12), 7421−7497.

(40) Li, M.; Xiao, Y.; Deng, P.; Yu, Y. Near-Infrared Absorbing Para-Azaquinodimethane Conjugated Polymers Synthesized via the Transition-Metal-Free Route toward Efficient Photothermal Conversion. *Rapid Commun.* **2024**, *45*, 2300648.

(41) Gong, X.; Tong, M.; Xia, Y.; Cai, W.; Moon, J. S.; Cao, Y.; Yu, G.; Shieh, C.-L.; Nilsson, B.; Heeger, A. J. High-Detectivity Polymer Photodetectors with Spectral Response from 300 Nm to 1450 Nm. *Science* **2009**, *325* (5948), 1665−1667.

(42) Kim, I. K.; Jo, J. H.; Lee, J.; Choi, Y. J. Detectivity Analysis for Organic Photodetectors. *Org. Electron.* **2018**, *57*, 89−92.

(43) Liu, G.; Li, T.; Zhan, X.; Wu, H.; Cao, Y. High-Sensitivity Visible-Near Infrared Organic Photodetectors Based on Non-Fullerene Acceptors. *ACS Appl. Mater. Interfaces* **2020**, *12* (15), 17769−17775.

(44) Trasatti, S. The Absolute Electrode Potential: An Explanatory Note. *Pure Appl. Chem.* **1986**, *58* (7), 955−966.

(45) Pommerehne, J.; Vestweber, H.; Guss, W.; Mahrt, R. F.; Bässler, H.; Porsch, M.; Daub, J. Efficient Two Layer Leds on a Polymer Blend Basis. *Adv. Mater.* **1995**, *7* (6), 551−554.

(46) Frisch, M. J.; et al. *Gaussian 16*, revision C.01; Gaussian, Inc.: Wallingford, CT, 2016.

(47) Wolfe, J. F.; Loo, B. H.; Arnold, F. E. Rigid-Rod Polymers. 2. Synthesis and Thermal Properties of Para-Aromatic Polymers with 2,6-Benzobisthiazole Units in the Main Chain. *Macromolecules* **1981**, *14* (4), 915−920.

(48) Wang, S.; Hong, W.; Ren, S.; Li, J.; Wang, M.; Gao, X.; Li, H. New Ladder-Type Conjugated Polymer with Broad Absorption, High Thermal Dtability, and Low Band Gap. *J. Polym. Sci. A. Polym. Chem.* **2012**, *50* (20), 4272−4276.

(49) Mosca, S.; Milani, A.; Castiglioni, C.; Hernández Jolín, V.; Meseguer, C.; López Navarrete, J. T.; Zhao, C.; Sugiyasu, K.; Ruiz Delgado, M. C. Raman Fingerprints of π-Electron Delocalization in Polythiophene-Based Insulated Molecular Wires. *Macromolecules* **2022**, *55* (9), 3458−3468.

(50) Tian, B.; Zerbi, G. Lattice Dynamics and Vibrational Spectra of Pristine and Doped Polypyrrole: Effective Conjugation Coordinate. *J. Chem. Phys.* **1990**, *92* (6), 3892−3898.

(51) Zerbi, G. Vibrational Spectroscopy of Conducting Polymers: Theory and Perspective. *Handbook of Vibrational Spectroscopy*; Chalmers, J. M., Griffiths, P. R., Eds.; 2007; DOI: 10.1002/9780470027325.s8920.

(52) Hernandez, V.; Castiglioni, C.; Del Zoppo, M.; Zerbi, G. Confinement Potential and π-Electron Delocalization in Polyconjugated Organic Materials. *Phys. Rev. B* **1994**, *50* (14), 9815−9823.

(53) Roberts, M. F.; Jenekhe, S. A. Lewis-Acid Coordination-Complexes of Polymers.3. Poly(Benzimidazobenzophenanthroline) Ladder and Semiladder Polymers. *Polymer* **1994**, *35* (20), 4313−4325.

(54) Batsanov, S. S. Van Der Waals Radii of Elements. *Inorg. Mater.* **2001**, 37, 871.

(55) Farmer, B. L.; Dudis, D. S.; Adams, W. W. Calculation of the Effects of Protonation on Rigid-Rod Polymers. *Polymer* **1994**, *35* (17), 3745−3751.

(56) Kim, H. G.; Kang, B.; Ko, H.; Lee, J.; Shin, J.; Cho, K. Synthetic Tailoring of Solid-State Order in Diketopyrrolopyrrole-Based Copolymers via Intramolecular Noncovalent Interactions. *Chem. Mater.* **2015**, *27* (3), 829−838.

(57) Li, Y.; Sonar, P.; Murphy, L.; Hong, W. High Mobility Diketopyrrolopyrrole (DPP)-Based Organic Semiconductor Materials for Organic Thin Film Transistors and Photovoltaics. *Energy Environ. Sci.* **2013**, *6* (6), 1684−1710.

(58) Guo, X.; Liao, Q.; Manley, E. F.; Wu, Z.; Wang, Y.; Wang, W.; Yang, T.; Shin, Y.-E.; Cheng, X.; Liang, Y.; Chen, L. X.; Baeg, K.-J.; Marks, T. J.; Guo, X. Materials Design via Optimized Intramolecular Noncovalent Interactions for High-Performance Organic Semiconductors. *Chem. Mater.* **2016**, *28* (7), 2449−2460.

(59) Tian, Y.-H.; Kertesz, M. Low-Bandgap Pyrazine Polymers: Ladder-Type Connectivity by Intramolecular S···N(Sp2) Interactions and Hydrogen Bonds. *Macromolecules* **2009**, *42* (7), 2309−2312.

(60) Brédas, J. L.; Beljonne, D.; Coropceanu, V.; Cornil, J. Charge-Transfer and Energy-Transfer Processes in π-Conjugated Oligomers and Polymers: A Molecular Picture. *Chem. Rev.* **2004**, *104* (11), 4971−5004.

(61) Zade, S. S.; Zamoshchik, N.; Bendikov, M. From Short Conjugated Oligomers to Conjugated Polymers. Lessons from Studies on Long Conjugated Oligomers. *Acc. Chem. Res.* **2011**, *44* (1), 14−24.

(62) Berry, G. C. Properties of an Optically Anisotropic Heterocyclic Ladder Polymer (BBL) in Dilute Solution. *J. Polym. Sci. Polym. Symp.* **1978**, *65* (1), 143−172.

(63) Berry, G. C.; Yen, S. P. Structure and Properties of a Heterocyclic Polymer. *Addition and Condensation Polymerization Processes* **1969**, *91*, 734−756.

(64) Yang, C. J.; Jenekhe, S. A. Conjugated Aromatic Polyimines. 2. Synthesis, Structure, and Properties of New Aromatic Polyazomethines. *Macromolecules* **1995**, *28* (4), 1180−1196.

(65) Wu, P.-T.; Kim, F. S.; Champion, R. D.; Jenekhe, S. A. Conjugated Donor-Acceptor Copolymer Semiconductors. Synthesis, Optical Properties, Electrochemistry, and Field-Effect Carrier Mobility of Pyridopyrazine-Based Copolymers. *Macromolecules* **2008**, *41* (19), 7021−7028.

(66) Leenaers, P. J.; Maufort, A. J. L. A.; Wienk, M. M.; Janssen, R. A. J. Impact of π-Conjugated Linkers on the Effective Exciton Binding Energy of Diketopyrrolopyrrole-Dithienopyrrole Copolymers. *J. Phys. Chem. C* **2020**, *124* (50), 27403−27412.

(67) Izquierdo, M. A.; Broer, R.; Havenith, R. W. A. Theoretical Study of the Charge Transfer Exciton Binding Energy in Semiconductor Materials for Polymer:Fullerene-Based Bulk Heterojunction Solar Cells. *J. Phys. Chem. A* **2019**, *123* (6), 1233−1242.

(68) Hedström, S.; Henriksson, P.; Wang, E.; Andersson, M. R.; Persson, P. Temperature-Dependent Optical Properties of Flexible Donor-Acceptor Polymers. *J. Phys. Chem. C* **2015**, *119* (12), 6453−6463.

(69) Gregory, S. A.; Hanus, R.; Atassi, A.; Rinehart, J. M.; Wooding, J. P.; Menon, A. K.; Losego, M. D.; Snyder, G. J.; Yee, S. K. Quantifying Charge Carrier Localization in Chemically Doped Semiconducting Polymers. *Nat. Mater.* **2021**, *20* (10), 1414−1421.

(70) Kim, N. Y.; Lee, T. S.; Lee, D. Y.; Oh, J. G.; Lee, K.; Kim, J. Y.; An, T. K.; Jeong, Y. J.; Jang, J.; Kim, Y.-H. Enhanced Doping Efficiency and Thermoelectric Performance of Diketopyrrolopyrrole-Based Conjugated Polymers with Extended Thiophene Donors. *J. Mater. Chem. C* **2021**, *9* (1), 340−347.

(71) Wu, L.; Li, H.; Chai, H.; Xu, Q.; Chen, Y.; Chen, L. Anion-Dependent Molecular Doping and Charge Transport in Ferric Salt-Doped P3HT for Thermoelectric Application. *ACS Appl. Electron. Mater.* **2021**, *3* (3), 1252−1259.

(72) Zeng, H.; Mohammed, M.; Untilova, V.; Boyron, O.; Berton, N.; Limelette, P.; Schmaltz, B.; Brinkmann, M. Fabrication of Oriented N-Type Thermoelectric Polymers by Polarity Switching in a DPP-Based Donor-Acceptor Copolymer Doped with FeCl3. *Adv. Electron. Mater.* **2021**, *7* (5), 2000880.

(73) Liang, Z.; Zhang, Y.; Souri, M.; Luo, X.; Boehm, A. M.; Li, R.; Zhang, Y.; Wang, T.; Kim, D.-Y.; Mei, J.; Marder, S. R.; Graham, K. R.

Influence of Dopant Size and Electron Affinity on the Electrical Conductivity and Thermoelectric Properties of a Series of Conjugated Polymers. *J. Mater. Chem. A* **2018**, *6* (34), 16495−16505.

(74) Geng, X.; Du, T.; Xu, C.; Liu, Y.; Deng, Y.; Geng, Y. Realizing P-Type and n-Type Doping of a Single Conjugated Polymer via Incorporation of a Thienoisatin-Terminated Quinoidal Unit. *Adv. Funct. Mater.* **2023**, *33* (28), 2300809.

(75) Tang, C. G.; Hou, K.; Leong, W. L. The Quest for Air Stability in Organic Semiconductors. *Chem. Mater.* **2024**, *36* (1), 28−53.

(76) Scholes, D. T.; Hawks, S. A.; Yee, P. Y.; Wu, H.; Lindemuth, J. R.; Tolbert, S. H.; Schwartz, B. J. Overcoming Film Quality Issues for Conjugated Polymers Doped with F4TCNQ by Solution Sequential Processing: Hall Effect, Structural, and Optical Measurements. *J. Phys. Chem. Lett.* **2015**, *6* (23), 4786−4793.

(77) Fontana, M. T.; Stanfield, D. A.; Scholes, D. T.; Winchell, K. J.; Tolbert, S. H.; Schwartz, B. J. Evaporation vs Solution Sequential Doping of Conjugated Polymers: F4TCNQ Doping of Micrometer-Thick P3HT Films for Thermoelectrics. *J. Phys. Chem. C* **2019**, *123* (37), 22711−22724.

(78) Wang, S.; Ruoko, T.-P.; Wang, G.; Riera-Galindo, S.; Hultmark, S.; Puttisong, Y.; Moro, F.; Yan, H.; Chen, W. M.; Berggren, M.; Müller, C.; Fabiano, S. Sequential Doping of Ladder-Type Conjugated Polymers for Thermally Stable n-Type Organic Conductors. *ACS Appl. Mater. Interfaces* **2020**, *12* (47), 53003−53011.

(79) Scholes, D. T.; Yee, P. Y.; McKeown, G. R.; Li, S.; Kang, H.; Lindemuth, J. R.; Xia, X.; King, S. C.; Seferos, D. S.; Tolbert, S. H.; Schwartz, B. J. Designing Conjugated Polymers for Molecular Doping: The Roles of Crystallinity, Swelling, and Conductivity in Sequentially-Doped Selenophene-Based Copolymers. *Chem. Mater.* **2019**, *31* (1), 73−82.

(80) Jacobs, I. E.; Aasen, E. W.; Oliveira, J. L.; Fonseca, T. N.; Roehling, J. D.; Li, J.; Zhang, G.; Augustine, M. P.; Mascal, M.; Moulé, A. J. Comparison of Solution-Mixed and Sequentially Processed P3HT:F4TCNQ Films: Effect of Doping-Induced Aggregation on Film Morphology. *J. Mater. Chem. C* **2016**, *4* (16), 3454−3466.

(81) Jha, M.; Mogollon Santiana, J.; Jacob, A. A.; Light, K.; Hong, M. L.; Lau, M. R.; Filardi, L. R.; Miao, H.; Gurses, S. M.; Kronawitter, C. X.; Mascal, M.; Moulé, A. J. Stability Study of Molecularly Doped Semiconducting Polymers. *J. Phys. Chem. C* **2024**, *128* (3), 1258−1266.

(82) Jacobs, I. E.; Moulé, A. J. Controlling Molecular Doping in Organic Semiconductors. *Adv. Mater.* **2017**, *29* (42), 1703063.

(83) Scheunemann, D.; Järsvall, E.; Liu, J.; Beretta, D.; Fabiano, S.; Caironi, M.; Kemerink, M.; Müller, C. Charge Transport in Doped Conjugated Polymers for Organic Thermoelectrics. *Chem. Phys. Rev.* **2022**, *3* (2), 021309.

(84) Wang, X.; Zhang, Z.; Li, P.; Xu, J.; Zheng, Y.; Sun, W.; Xie, M.; Wang, J.; Pan, X.; Lei, X.; Wang, J.; Chen, J.; Chen, Y.; Wang, S.-J.; Lei, T. Ultrastable N-Type Semiconducting Fiber Organic Electrochemical Transistors for Highly Sensitive Biosensors. *Adv. Mater.* **2024**, *36* (24), 2400287.

(85) Yang, C.; Stoeckel, M.; Ruoko, T.; Wu, H.; Liu, X.; Kolhe, N.; Wu, Z.; Puttisong, Y.; Musumeci, C.; Massetti, M.; Sun, H.; Xu, K.; Tu, D.; Chen, W.; Woo, H.; Fahlman, M.; Jenekhe, S.; Berggren, M.; Fabiano, S. A High-Conductivity n-Type Polymeric Ink for Printed Electronics. *Nat. Commun.* **2021**, *12*, 2354.

(86) West, S. M.; Tran, D. K.; Guo, J.; Chen, S. E.; Ginger, D. S.; Jenekhe, S. A. Phenazine-Substituted Poly(Benzimidazobenzophenanthrolinedione): Electronic Structure, Thin Film Morphology, Electron Transport, and Mechanical Properties of an n-Type Semiconducting Ladder Polymer. *Macromolecules* **2023**, *56* (5), 2081−2091.

(87) Tran, D. K.; West, S. M.; Speck, E. M. K.; Jenekhe, S. A. Observation of Super-Nernstian Proton-Coupled Electron Transfer and Elucidation of Nature of Charge Carriers in a Multiredox Conjugated Polymer. *Chem. Sci.* **2024**, *15* (20), 7623−7642.

(88) Lim, D.-H.; Ha, J.-W.; Choi, H.; Yoon, S. C.; Lee, B. R.; Ko, S.-J. Recent Progress of Ultra-Narrow-Bandgap Polymer Donors for NIR-Absorbing Organic Solar Cells. *Nanoscale Adv.* **2021**, *3* (15), 4306−4320.

(89) Bundgaard, E.; Krebs, F. C. Low Band Gap Polymers for Organic Photovoltaics. *Sol. Energy Mater. Sol. Cells* **2007**, *91* (11), 954−985.

(90) Chen, L. X. Organic Solar Cells: Recent Progress and Challenges. *ACS Energy Lett.* **2019**, *4* (10), 2537−2539.

Supporting Information

Conjugated Ladder Poly(thienobenzothiazine): Synthesis, Electronic Structure, Optical Properties, and Electrical Conductivity of a Narrow Bandgap p-Type Semiconducting Polymer

Sarah M. West,[a] Duyen K. Tran,[b] Werner Kaminsky,[a] and Samson A. Jenekhe*[a,b]

[a] Department of Chemistry, University of Washington, Seattle, Washington 98195-1750, United States of America.

[b] Department of Chemical Engineering, University of Washington, Seattle, Washington 98195-1750, United States of America.

TABLE OF CONTENTS

I. Additional Experimental Methods

Fabrication of Freestanding Films.

Freestanding films of LTBT were prepared on initial supporting glass substrates using a similar procedure as described above where the polymer solution (15 mg/mL) drop-cast onto a hot substrate and baked overnight at 120˚C. Instead of additional annealing at higher temperature, the thin films were then slowly cooled down to room temperature and submerged in water. Thus, films can be peeled from the supporting substrate, floated on water, lifted off using a copper wire, and dried at 120˚C to form freestanding films. These freestanding films were used for further characterizations (FTIR and Raman Spectroscopies).

Experimental Details of X-Ray Crystallography

A red needle, measuring 0.60 x 0.04 x 0.005 mm^3 was mounted on a loop with oil. Crystal diffraction data was collected at -173˚C on a Bruker APEX II single crystal X-ray diffractometer, Mo-radiation, equipped with a Miracol X-ray optical collimator. Crystal-to-detector distance was 40 mm and exposure time was 30 seconds per frame for all sets. The scan width was 0.75˚. Data collection was 100.0% complete to 25^o in □. A total of 10370 reflections were collected covering the indices, h = -21 to 21, k = -25 to 25, l = -4 to 4. 2698 reflections were symmetry independent and the R_{int} = 0.1668 indicated that the data was of better than average quality (0.07). Indexing and unit cell refinement indicated an orthorhombic lattice. The space group was found to be $Pna2_1$ (No. 33). The data was integrated and scaled using SAINT, SADABS within the APEX2 software package by Bruker.[1] Solution by direct methods (SHELXT[2-3] or SIR97[4-5]) produced a complete heavy atom phasing model consistent with the proposed structure. The structure was completed by difference Fourier synthesis with SHELXL.[6-7] Scattering factors are from Waasmair and Kirfel[8]. Hydrogen atoms were placed in geometrically idealised positions and constrained to ride on their parent atoms with C---H distances in the range 0.95-1.00 Angstrom. Isotropic thermal parameters U_{eq} were fixed such that they were $1.2U_{eq}$ of their parent atom Ueq for CH's and $1.5U_{eq}$ of their parent atom U_{eq} in case of methyl groups. All non-hydrogen atoms were refined anisotropically by full-matrix least-squares.

II. Supporting Figures

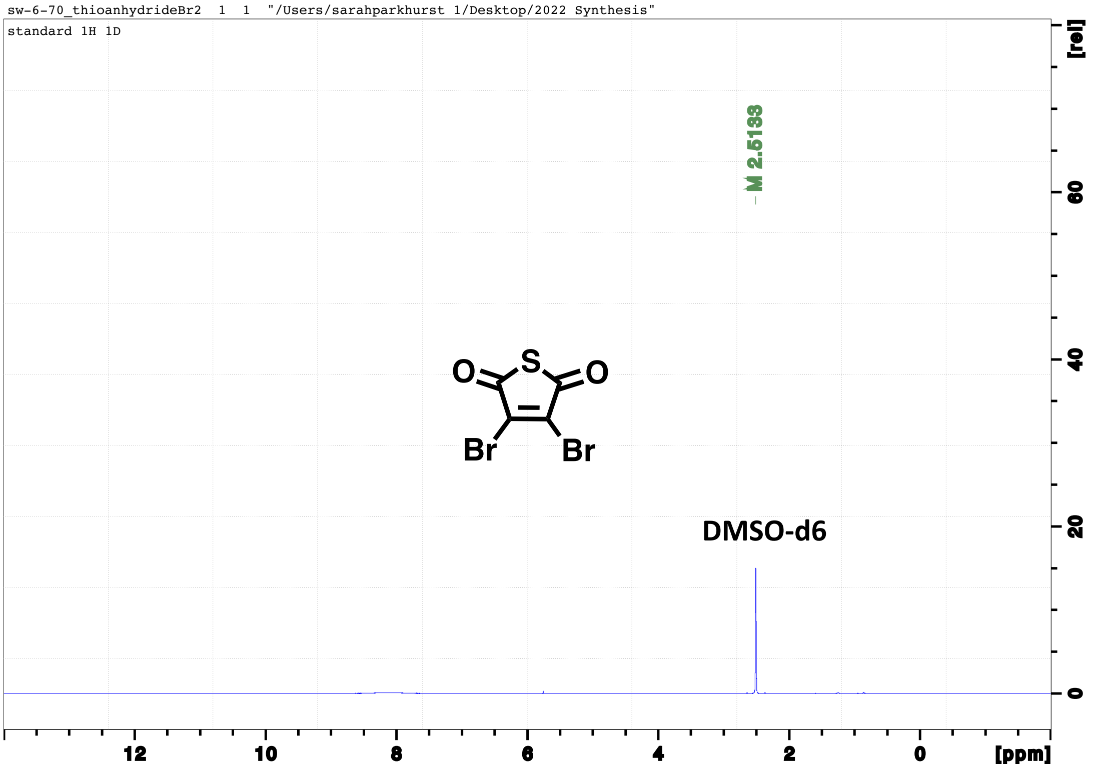

Figure S1. Proton NMR of the monomer 3,4-dibromothiophene-2,5-dione in DMSO-d6.

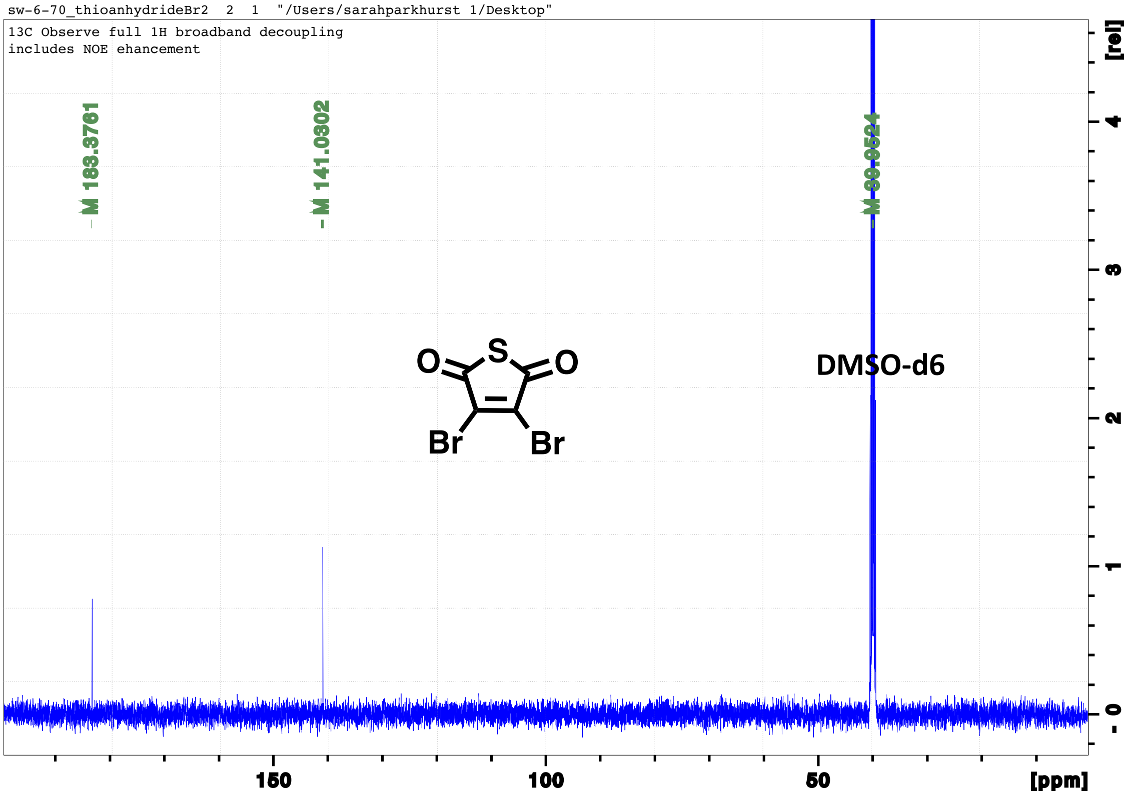

Figure S2. Carbon NMR of monomer 3,4-dibromothiophene-2,5-dione in DMSO-d6.

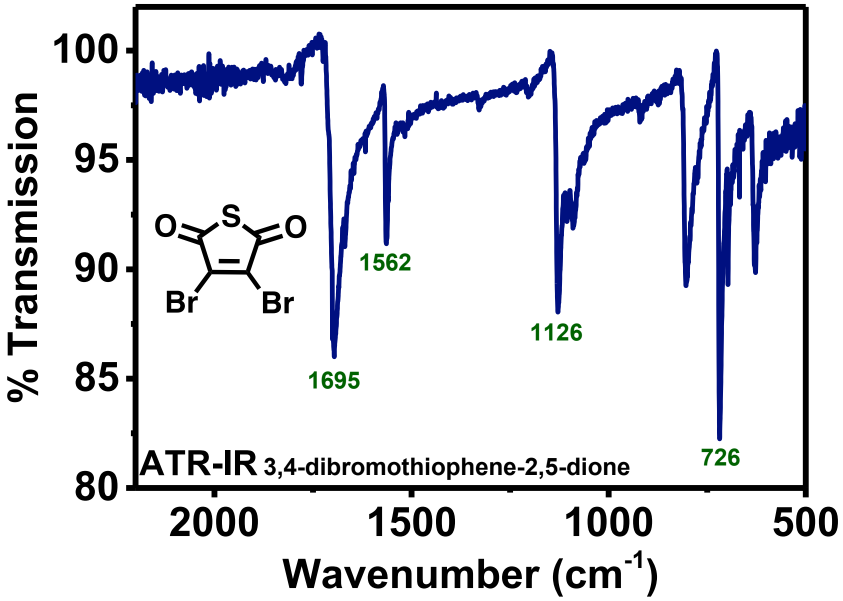

Figure S3. Attenuated Total Reflectance Fourier-transform Infrared (ATR-FTIR) spectrum of the neat monomer, 3,4-dibromothiophene-2,5-dione.

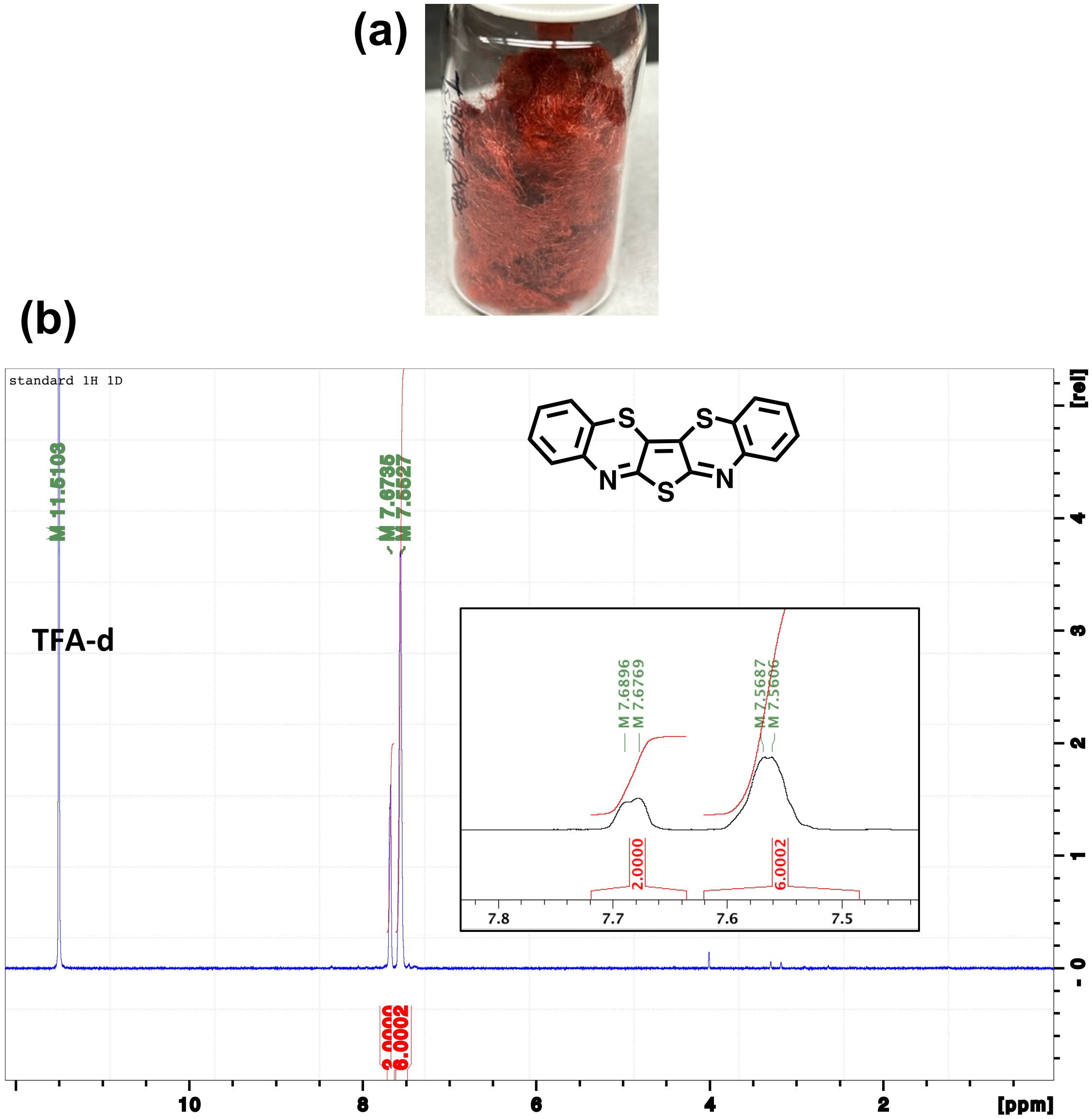

Figure S4. (a) Needles of TBBT. (b) Proton NMR of TBBT in TFA-d. Insert shows the peak integration for the benzene moiety.

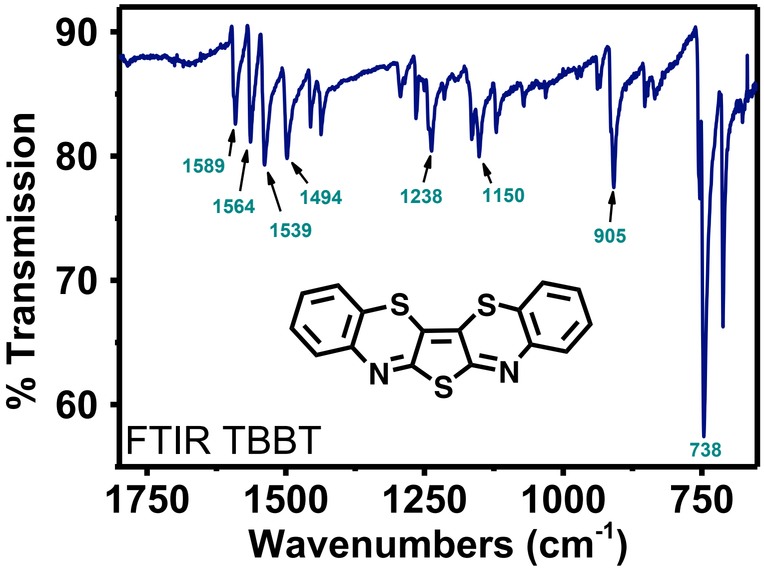

Figure S5. FTIR spectrum of TBBT.

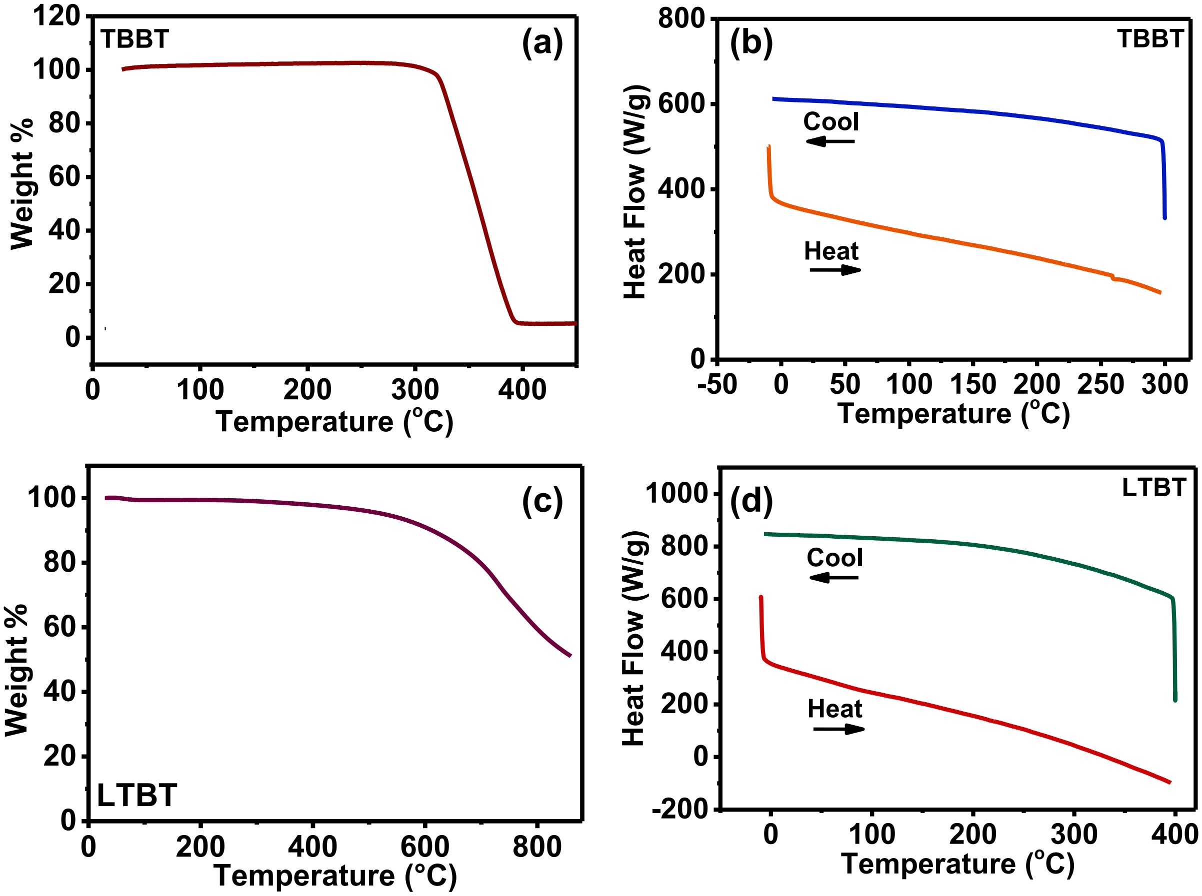

Figure S6. Thermal gravimetric analysis (TGA) scans of (a) TBBT and (c) LTBT under nitrogen at a scan rate of 10˚C/min. Differential scanning calorimetry (DSC) scans of (b) TBBT and (d) LTBT at a scan rate of 10˚C/min under nitrogen.

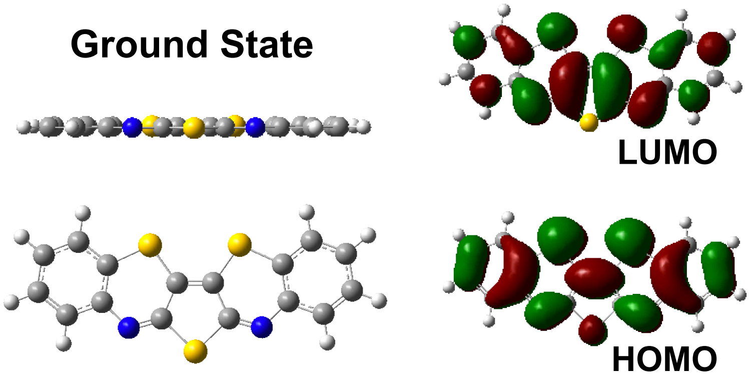

Figure S7. Ground state geometry and molecular orbital distributions of TBBT calculated using DFT at B97XD/6-31G(d,p) level of theory.

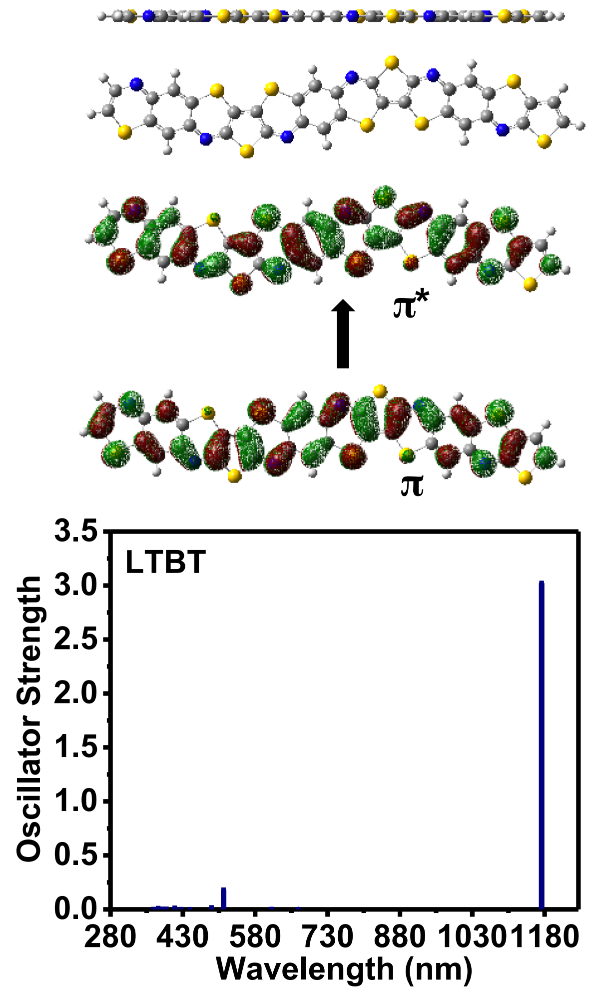

Figure S8. Excited state geometry and simulated vertical excitations of the gas phase LTBT oligomer, and the corresponding hole and electron wavefunctions for the lowest energy transition (π-π*) at 1170 nm calculated using TD-DFT B97XD/6-31G(d,p) level of theory for n=12 excited states ($_{max}$ = 1170 nm).

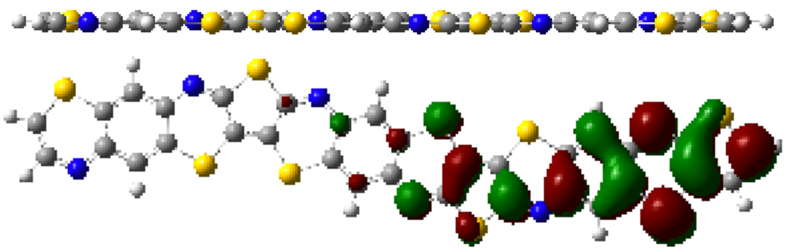

Figure S9. Cationic LTBT oligomer geometry and polaron orbital distribution calculated at the DFT at □B97XD/6-31G(d,p) level of theory.

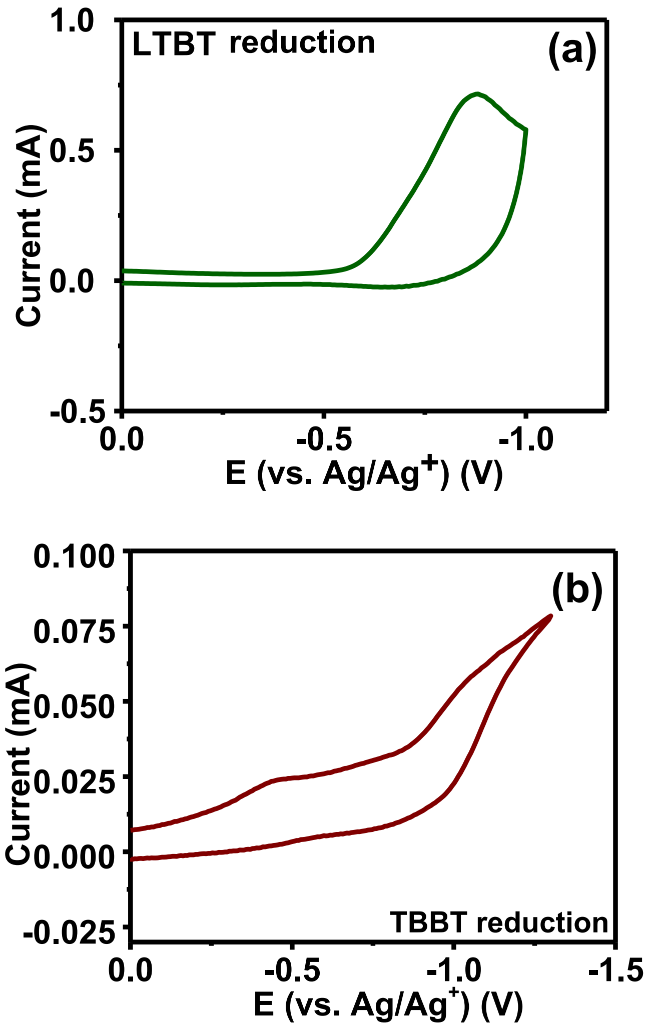

Figure S10. The reduction scans of (a) LTBT and (b) TBBT in 0.1 M Bu_4NPF_6 acetonitrile solution vs. Ag/Ag^+. The scan rate was 100 mV/s.

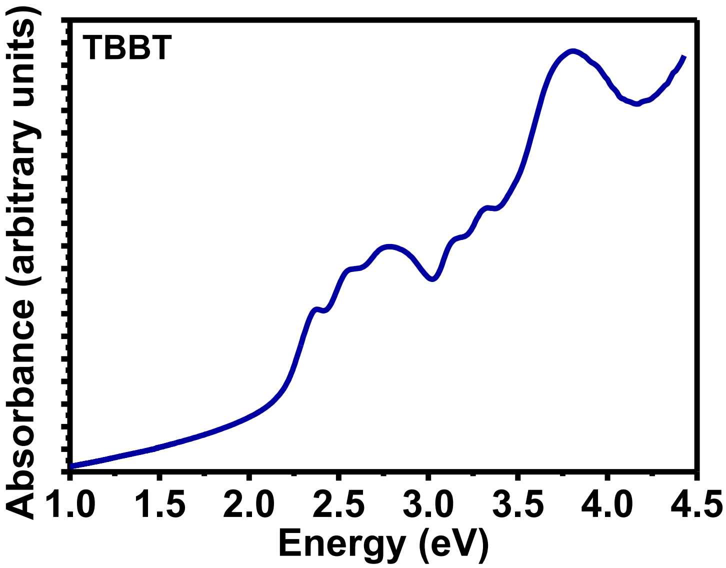

Figure S11. Thin film absorption spectra of TBBT plotted vs. eV to determine the optical bandgap from the onset of absorption.

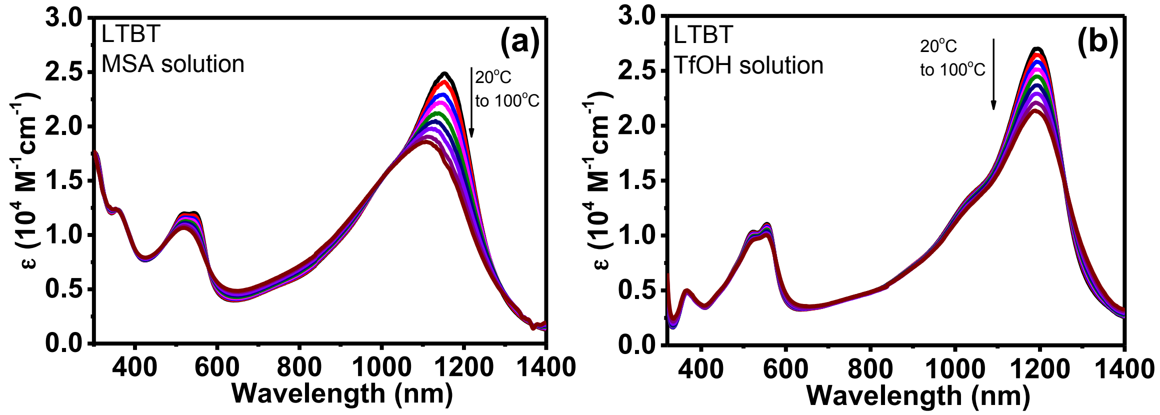

Figure S12. Optical absorption spectra of LTBT in (a) dilute (10^{-5} M) MSA solution (□$_{max}$ = 1151 nm) and (b) triflic acid solution (□$_{max}$ = 1192 nm).

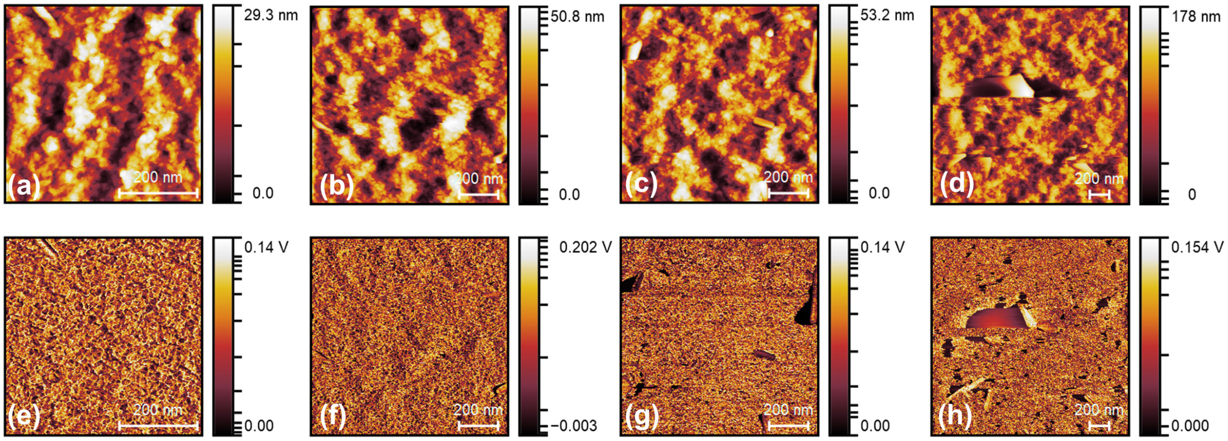

Figure S13. (a - d) Atomic force microscopy (AFM) height images of neat LTBT thin films deposited on glass; (e -h) AFM phase images of neat LTBT films.

III. Supporting Tables.

Table S1. Fourier-Transform Infrared Spectroscopy (FTIR) and Raman Absorption Bands of LTBT Freestanding Films and Their Peak Assignments.

FTIR Absorption Band (cm^{-1})	Raman Absorption Band (cm^{-1})	Assignment
1601	1614, 1462	ν(C=C/C-C)/(Я band), carbon-carbon stretches
1534	1592, 1530	ν(C=N), imine carbon-nitrogen stretches
1443, 1300	1487	Thiophene stretches, mixed aromatic stretches
1226	-	ν(C-N), carbon-nitrogen stretch
1150	1073	ν(C-S), carbon-sulfur stretch
908, 800	1268, 1155	Intraring vibrations

Table S2. Fourier-Transform Infrared Spectroscopy (FTIR) Absorption Bands of TBBT Needles and Their Peak Assignments.

FTIR Absorption Band (cm^{-1})	Assignment
1589, 1564	ν(C=C), carbon-carbon stretch
1539	ν(C=N), imine carbon-nitrogen stretch
1494, 1456, 1291	Thiophene stretches, mixed aromatic stretches
1238	ν(C-N), carbon-nitrogen stretch
1150	ν(C-S), carbon-sulfur stretch
905, 738	Mixed skeletal vibrations

Table S3. Crystallographic data for TBBT.

Empirical formula	C16 H8 N2 S3	
Formula weight	324.42	
Temperature	100(2) K	
Wavelength	0.71073 Å	
Crystal system	Orthorhombic	
Space group	P n a 2_1	
Unit cell dimensions	a = 17.198(9) Å	□= 90°.
	b = 20.222(12) Å	□= 90°.
	c = 3.782(2) Å	□= 90°.
Volume	1315.3(13) Å^3	
Z	4	
Density (calculated)	1.638 Mg/m^3	
Absorption coefficient	0.555 mm^{-1}	
F(000)	664	
Crystal size	0.600 x 0.040 x 0.005 mm^3	
Theta range for data collection	1.554 to 26.533°.	
Index ranges	-21<=h<=21, -25<=k<=25, -4<=l<=4	
Reflections collected	10370	
Independent reflections	2698 [R(int) = 0.1668]	
Completeness to theta = 25.000°	100.0 %	

Refinement method	Full-matrix least-squares on F^2
Data / restraints / parameters	2698 / 1 / 191
Goodness-of-fit on F^2	0.976
Final R indices [I>2sigma(I)]	R1 = 0.0524, wR2 = 0.1000
R indices (all data)	R1 = 0.0990, wR2 = 0.1168
Absolute structure parameter	-0.08(12)
Extinction coefficient	0.012(2)
Largest diff. peak and hole	0.485 and -0.473 e.Å^{-3}

Table S4. Atomic coordinates (x 10^4) and equivalent isotropic displacement parameters (Å^{2}x 10^3) for TBBT. U(eq) is defined as one third of the trace of the orthogonalized U^{ij} tensor.

	x	y	z	U(eq)
S(2)	4868(1)	7032(1)	7865(6)	23(1)
S(3)	5706(1)	5535(1)	7436(5)	24(1)
S(1)	7167(1)	7077(1)	3171(6)	25(1)
N(1)	6124(3)	8017(3)	4460(15)	24(1)
N(2)	7371(3)	5782(3)	3676(15)	22(1)
C(5)	4020(4)	8870(3)	8030(20)	25(2)
C(4)	4117(4)	8196(3)	8362(19)	23(2)
C(3)	4803(4)	7890(3)	7240(18)	20(2)
C(2)	5782(4)	6874(3)	6129(18)	23(2)
C(10)	6129(4)	6264(3)	5930(18)	20(2)
C(11)	6436(4)	4962(3)	6281(18)	23(2)
C(12)	6291(4)	4303(3)	7160(20)	26(2)
C(13)	6850(4)	3820(3)	6410(20)	27(2)
C(14)	7551(4)	3989(4)	4839(19)	29(2)
C(6)	4608(4)	9241(4)	6472(19)	31(2)
C(7)	5294(4)	8947(3)	5334(19)	26(2)
C(8)	5407(4)	8260(3)	5730(18)	23(2)
C(1)	6271(4)	7395(3)	4733(18)	22(2)
C(9)	6896(4)	6264(3)	4347(18)	23(2)
C(16)	7149(4)	5136(3)	4651(18)	24(2)
C(15)	7693(4)	4638(3)	3949(19)	25(2)

IV. Supporting References

1. Bruker **2007,** APEX2 (Version 2.1-4), SAINT (version 7.34A), SADABS (version 2007/4), BrukerAXS Inc, Madison, Wisconsin, USA.
2. Sheldrick, G. M. A Short History of SHELX. *Acta. Cryst.* **2008**, A64, 112-122.
3. Sheldrick, G. M. SHELXT - Integrated Space-Group and Crystal-Structure Determination. *Acta. Cryst.* **2015**, A71, 3-8.
4. Altomare, A.; Burla, C.; Camalli, M.; Cascarano, G. L.; Giacovazzo, C.; Guagliardi, A.; Moliterni, A. G. G.; Polidori, G.; Spagna, R. SIR97: A New Tool for Crystal Structure Determination and Refinement *J. Appl. Crystallogr*. **1999** *32***,** 115-119.
5. Altomare, A.; Cascarano, G. L.; Giacovazzo, C.; Guagliardi, A. Completion and Refinement of Crystal Structures with SIR 92. *J. Appl. Crystallogr.* **1993** *26***,** 343-350.
6. Sheldrick G. M. SHELXL-97, Program for the Refinement of Crystal Structures. **1997**, University of Göttingen, Germany.
7. Sheldrick G. M. Crystal Structure Refinement with SHELXL. *Acta Cryst*. **2015**, C71, 3–8.
8. Waasmaier, D.; Kirfel, A. New Analytical Scattering Factor Functions for Free Atoms and Ions. *Acta. Cryst. A.* **1995**, *51*, 416-430.